Lithos 277 (2017) 210–227

Contents lists available at ScienceDirect

Lithos

journal homepage: www.elsevier.com/locate/lithos

F-rich strongly peraluminous A-type magmatism in the pre-Andean foreland Sierras Pampeanas, Argentina: Geochemical, geochronological, isotopic constraints and petrogenesis

Matías M. Morales Cámera [a,*], Juan A. Dahlquist [a], Miguel A.S. Basei [b], Carmen Galindo [c], Mario da Costa Campos Neto [b], Nicolás Facetti [d]

[a] CICTERRA-CONICET-UNC, Av. Vélez Sarsfield 1611, Pab. GeoL., X5016CGA Córdoba, Argentina
[b] Instituto de Geociências da Universidade de São Paulo, Rua do Lago 562, 05508-080 São Paulo, SP, Brazil
[c] Departamento de Petrología y Geoquímica, Universidad Complutense, 28040 Madrid, Spain
[d] Regional Noroeste, Comisión Nacional de Energía Atómica, Avenida Bolivia 4650 - 1° Piso, 4400 Salta, Argentina

ARTICLE INFO

Article history:
Received 3 February 2016
Accepted 27 October 2016
Available online 4 November 2016

Keywords:
Strongly peraluminous Carboniferous A-type granites
Geochronological
Geochemistry
Isotopes
Pre-Andean margin
Oxidized A-type granites

ABSTRACT

The petrogenetic nature of A-type granites is a controversial problem. The Vinquis batholith in the Sierras Pampeanas of Argentina contains unusual F-rich and strongly peraluminous A-type monzogranites. A new LA-MC-ICP-MS U–Pb zircon crystallization age of 355 ± 7 Ma indicates emplacement in latest Devonian or earliest Carboniferous time, overlapping with extensive metaluminous A-type magmatism in the area. The monzogranites have a restricted range of SiO_2 content (71.5–74.8 %), they are poor in Ca (0.54–1.4% CaO) and rich in FeO^t, with relatively high $FeO^t/(FeO^t+MgO)$ values ranging from 0.77 to 0.86 (average = 0.80) Both $[FeO^t/(FeO^t+MgO)]$ vs. SiO_2 and $[(Na_2O+K_2O)-CaO]$ vs. SiO_2 plots indicate ferroan and alkali-calcic signatures typical of A-type granitoids. The samples have $MgO/TiO_2 > 1.2$ and are moderately enriched in total alkalis (average 8.18%), with high K_2O/Na_2O values of 1.40–2.24. The granites are strongly peraluminous, with ASI (molar $Al_2O_3/[CaO + Na_2O + K_2O]$) values of 1.2 to 1.3. The high P_2O_5 content (0.23–0.37%) is distinctive and close to values reported for other Paleozoic F-rich peraluminous A-type granites in the Sierras Pampeanas. They have moderate contents of high field strength elements (e.g., Zr, Nb, Th, Y, etc.) and moderately fractionated to flat REE patterns $[(La/Yb)_N$ in the range 4.8–19.6] showing significant negative Eu anomalies ($Eu/Eu^* = 0.41$). Biotite has a distinctive composition, with relatively high $Fe^{2+}/(Fe^{2+} + Mg)$ ratios (0.61–0.74) and high F (0.55–1.42 wt.%) content. Together with the whole-rock chemistry this may be useful in identifying strongly peraluminous A-type granites. In addition, the Rb/Sr vs. Th + Zr + Ce diagram may be an appropriate discriminant between metaluminous and peralkaline A-type granites, strongly peraluminous A-type granites and strongly peraluminous orogenic granites. The geochemical evidence indicates that differentiation of the granitic rocks occurred by mineral fractionation from a F-rich peraluminous parental magma, dominant of plagioclase, K-feldspar, biotite, and accessory minerals such as zircon, monazite, xenotime, and oxides. The peraluminous composition and isotope data ($\varepsilon_{Hf,355}$ and $\varepsilon_{Nd,355}$ ranging from −9.5 to −1.5 and −6.1 to −7.8, respectively), together with abundant inherited Ordovician and Cambrian zircon, strongly suggest a dominantly metasedimentary source. The whole-rock and biotite compositions indicate that the Vinquis batholith crystallized under mainly oxidizing conditions, whereas Early Carboniferous metaluminous to weakly peraluminous A-type granites of the Sierras Pampeanas crystallized under dominantly reduced conditions.

1. Introduction

A-type granites have distinct mineralogical and geochemical characteristics. However, their genesis has been controversial, leading to much discussion over the past 30 years (e.g., Bonin, 2007; Dall'Agnol et al., 2012; Frost and Frost, 2011; Papoutsa et al., 2015; Martin, 2006 and references therein). In general, petrogenetic models for A-type granites commonly invoke igneous source rocks (e.g., Dall'Agnol and Oliveira, 2007; Papoutsa et al., 2015; Patiño Douce, 1997), and there is limited knowledge about the petrogenesis of peraluminous A-type granites (Dahlquist et al., 2014 and references therein).

Many authors have stressed the variable petrogenetic nature of A-type granites (e.g., Dahlquist et al., 2010a; Dahlquist et al., 2014; Dall'Agnol and Oliveira, 2007; Eby, 1992; Frost and Frost, 2011; King et al., 1997; Martin, 2006; Patiño Douce, 1999), which reflects contrasts

* Corresponding author.
E-mail address: matiasmmoralesc@gmail.com (M.M. Morales Cámera).

http://dx.doi.org/10.1016/j.lithos.2016.10.035
0024-4937/

in magma sources and petrological processes. The relevance of oxidized, magnetite-series A-type granites and their differences compared to reduced, ilmenite-series rapakivi granites have been demonstrated in central and southwestern United States (Anderson and Bender, 1989; Anderson and Morrison, 1992, 2005; Anderson and Smith, 1995; Barnes et al., 2002) and the eastern Amazonian craton (Dall'Agnol et al., 1997a, 1999a, b, c, 2005; Rämö et al., 2002).

Anderson and Morrison (1992, 1998) reported the presence of Mesoproterozoic anorogenic A-type granites in the USA, which were divided in three large groups: i) low-fO_2, metaluminous ilmenite granites, ii) high-fO_2, metaluminous magnetite granites and iii) two-mica (peraluminous) granites. This classification has been discussed by a number of workers (e.g., Anderson and Morrison, 2005; Dall'Agnol and Oliveira, 2007; Johansson et al., 2016; Wang et al., 2015). In particular, Dall'Agnol and Oliveira (2007) studied Paleoproterozoic A-type granites in the eastern Amazonian craton and concluded that synchronous A-type granitic suites evolved in varying fO_2 conditions resulting in oxidized and reduced A-type granites.

Peraluminous A-type granites contain biotite or two micas, usually with aluminous phases such as sillimanite (Anderson and Thomas, 1985). However, these granites have been named as weakly peraluminous or aluminous A-type granites because their ASI (molar ratios of $(Al_2O_3/[CaO + Na_2O + K_2O])$ value is generally ≤1.1 (e.g., Anderson and Bender, 1989; Anderson and Thomas, 1985; Frost and Frost, 2011; King et al., 1997; Wang et al., 2015). Anderson and Morrison (2005) noted that these granites and metaluminous magnetite granites crystallized under oxidizing conditions, whereas metaluminous ilmenite granites crystallized under reduced conditions. As noticed by some authors (e.g., Anderson and Morrison, 1992, 2005; Dall'Agnol and Oliveira, 2007), oxidized A-type granites retain A-type characteristics, but they are less enriched in LILE and some HFSE, and have the lowest Fe/Mg and K/Na, and the highest $\delta^{18}O$ values. Thus, oxidized A-type granites have less typical A-type geochemical signature than those A-type granites that crystallized under reduced conditions (Dall'Agnol and Oliveira, 2007).

To the best of our knowledge, peraluminous A-type granites significantly enriched in Al (ASI > 1.1; i.e., strongly peraluminous) have been little discussed in the literature, although recently they have been more widely reported (e.g., Dahlquist et al., 2010b, Dahlquist et al., 2014, 2016; Feng et al., 2014; Shellnutt and Zhou, 2007; Sun et al., 2011; Xia et al., 2012). Although the geochemistry, the source and the resultant mineralogy of these rocks are diverse, they were all generated in a dominantly extensional tectonic regime.

A general conclusion (e.g. Barker et al., 1975; Dahlquist et al., 2010a; Eby, 1990) was that A-type magmas represent variable mixtures of two end member sources: asthenospheric mantle and continental crust. Variations in the mixing ratios lead to different subtypes of A-type granite, so that strongly peraluminous A-type granites could be mostly (or entirely) derived from a supracrustal source.

Recently, some authors (e.g., Dahlquist et al., 2015, 2016; Papoutsa et al., 2015; Shellnutt and Zhou, 2007) have noted that metaluminous to weakly peraluminous and strongly peraluminous A-type granitoids can be emplaced contemporaneously. In the pre-Andean margin of Gondwana (now Eastern Sierras Pampeanas) both strongly peraluminous and metaluminous to weakly peraluminous A-type granites were synchronously emplaced during the Early Carboniferous, ranging from 357 to 322 Ma (Dahlquist et al., 2016).

This study is a contribution to the understanding of the A-type magmatism focusing on the strongly peraluminous A-type granites. We present whole-rock chemistry data including major and trace element, mineral compositions and Sm-Nd isotope data for granitic rocks collected mainly from the eastern region of the Vinquis batholith located in the foreland of the pre-Andean margin of Gondwana (present-day Eastern Sierras Pampeanas of Argentina). In addition, a LA-MC-ICP-MS U–Pb zircon crystallization age is reported here, establish an Early Carboniferous age for the emplacement of the studied granitic rocks. Hf isotope data from dated magmatic zircon together with whole-rock Sm-Nd data are used to constrain the source of the parental magma. We use our data to assess the petrogenesis of this strongly peraluminous A-type granite.

2. Geological setting

The proto-Andean margin of Gondwana is an accretionary margin/orogen that has been active from at least the Early Ordovician to the present (Cawood, 2005). This has led to the formation of different plutonic rocks during the Palaeozoic (e.g., Dahlquist et al., 2013 and references therein).

In particular, the Sierras Pampeanas of Argentina (Fig. 1) are a series of mountainous ranges with a singular record of the magmatic activity that developed in this accretionary margin of Gondwana because they were strongly uplifted from Miocene times to the present (e.g., Jordan and Allmendinger, 1986). This elevation process was the result of a flat subduction event in an active margin setting (Ramos et al., 2002).

The Paleozoic igneous rocks were generated in four main magmatic events: (a) *Pampean magmatism* (latest Neoproterozoic-mid Cambrian; Iannizzotto et al., 2013; Rapela et al., 1998, 2007; Schwartz et al., 2008; Sims et al., 1998), (b) *Famatinian magmatism* (early-mid Ordovician Casquet et al., 2012; Dahlquist et al., 2008; Ducea et al., 2010; Otamendi et al., 2012; Pankhurst et al., 1998, 2000; Rapela et al., 2008a), (c) *Achalian magmatism* (mid-late Devonian; Dahlquist et al., 2014; Dorais et al., 1997; Rapela et al., 2008b; Sims et al., 1998; Siegesmund et al., 2004; Stuart-Smith et al., 1999), and (d) *Early Gondwana magmatism* (early Carboniferous; Alasino et al., 2012; Dahlquist et al., 2010a; Dahlquist et al., 2006, 2015, 2016; Grosse et al., 2009).

Our understanding of the petrogenesis of the Carboniferous granites in the Sierras Pampeanas has been improved in the last years (e.g., Alasino et al., 2012; Dahlquist et al., 2010a, Dahlquist et al., 2013, 2015, 2016; Grosse et al., 2009; and references therein). Thus, the studies reveal that undeformed Early Carboniferous metaluminous to weakly peraluminous A-type granites were mostly emplaced at shallow depth and are dominated by facies with K-feldspar megacrysts and that affect host rocks only locally (Dahlquist et al., 2010a). They form relatively small, isolated, subcircular plutons scattered throughout the Eastern Sierras Pampeanas, without any obvious spatial arrangement (Fig. 1).

In the studied region (central-northwestern Argentina, Fig. 1), Early Carboniferous metaluminous to weakly peraluminous A-type granites ranging in age from 322 to 357 Ma (Dahlquist et al., 2013) were emplaced within the continent (now the Eastern Sierras Pampeanas), away from an active plate margin (Alasino et al., 2012). Simultaneously, calc-alkaline granites were emplaced to the west, in the present-day Western Sierras Pampeanas and Cordillera Frontal (Dahlquist et al., 2015 and references therein). Thus, a geological setting similar to that postulated by Alasino et al. (2012, Fig. 12) is assumed here, including synchronous calc-alkaline and retro-arc A-type magmatism. Recently, Dahlquist et al. (2016) reported the presence of Early Carboniferous (336 Ma) strongly peraluminous A-type granite in Sierras de Córdoba (Fig. 1) and suggested that Early Carboniferous peraluminous and metaluminous A-type plutons were synchronously emplaced in the foreland pre-Andean margin of Gondwana.

The Early Carboniferous plutons were emplaced in metamorphic and igneous rocks produced during the development of Pampean and Famatinian orogenies. The Pampean orogeny has been associated with a calc-alkaline subduction-related magmatism (Iannizzotto et al., 2013 and references therein) followed by continent–continent collision in Early Cambrian time (Rapela et al., 2007 and reference therein) leading to a coeval granulite facies metamorphism and S_2 deformation. The Famatinian orogeny is associated with an extended Early Middle Ordovician magmatic arc (Dahlquist et al., 2013; Pankhurst et al., 1998), where the magmas were emplaced at mid-crustal levels leading to the

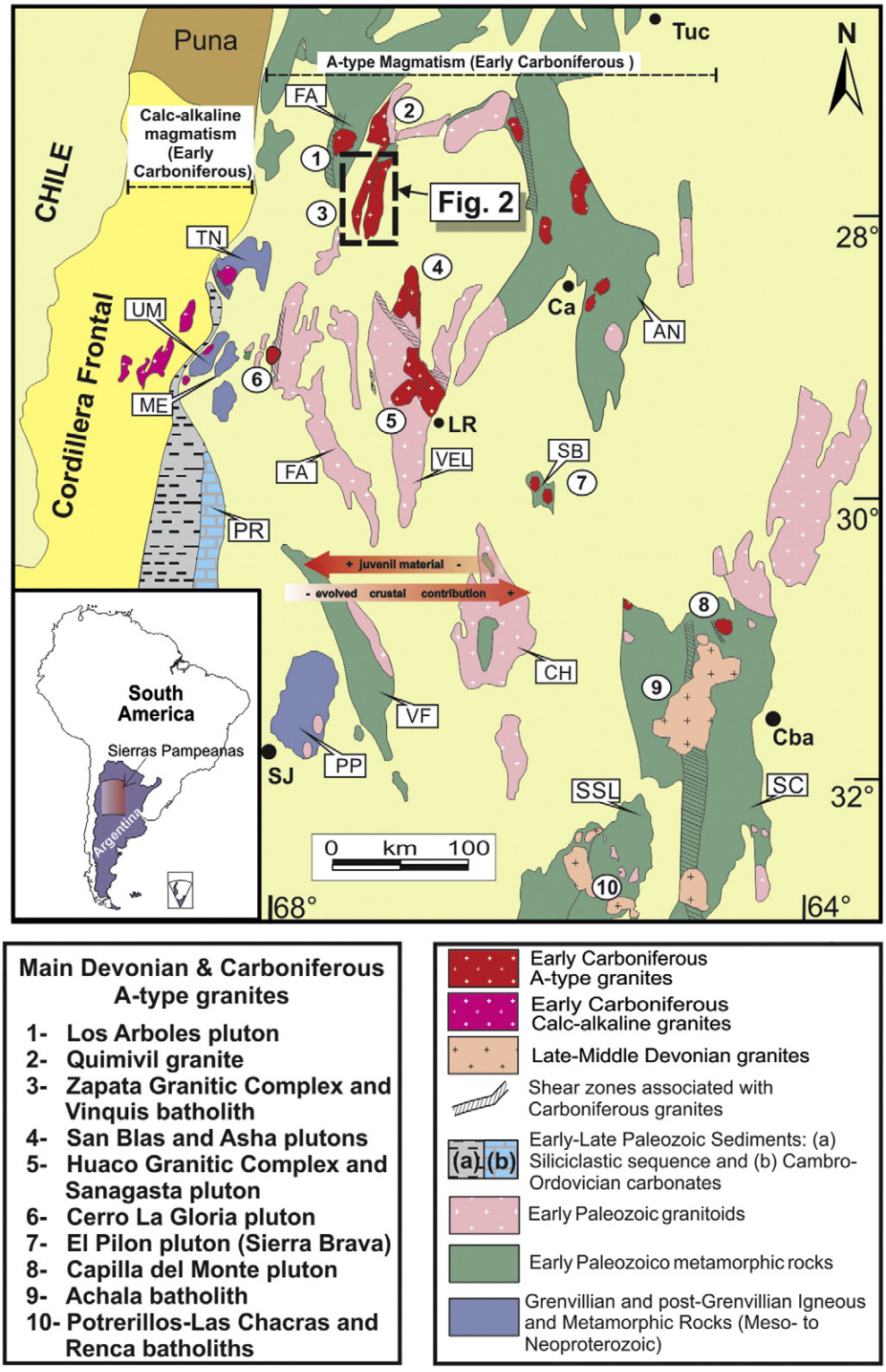

Fig. 1. Schematic geological map of west-central Argentina (Sierras Pampeanas) and the location of the studied region. Main Devonian and Carboniferous A-type granites in Sierras Pampeanas are located in the map. The red arrows indicating the participation of juvenile or continental material are applicable to the Carboniferous magmatism. Abbreviations: Tucumán (Tuc), La Rioja (LR), San Juan (SJ), Catamarca (Ca) and Córdoba (Cba). Main ranges: Sierra de Fiambala (FA), Sierra de Toro Negro (TN), Sierra de Umango (UM), Sierra de Ancasti (AN), Sierras de Maz-Espinal (ME), Sierra Brava (SB), Sierra de Velasco (VEL), Sierra de Famatina (FA), Precordillera (PR), Sierras de Chepes (CH), Sierra de Valle Fértil (VF), Sierra de Pie de Palo (PP), Sierra de Córdoba (SC) and Sierra de San Luis (SSL). Inset: rectangle defining study area displayed in Fig. 2.
(Modified from Alasino et al., 2012.)

formation of metamorphic rocks in the upper-amphibolite- to granulite-facies (Alasino et al., 2016; Otamendi et al., 2012). These Ordovician granites are typically affected by shear zones whereas the Early Carboniferous granites truncate these shear zones without ever being cut by them (e.g., Dahlquist et al., 2010a; Dahlquist et al., 2006; Larrovere et al., 2016; Miller and Söllner, 2005).

The Sierra of Vinquis in the south-central part of Catamarca province largely consists of a granitic batholith with an areal

extent of approximately 360 km^2. Various Early Carboniferous granitic complexes or plutons also crop out in the region. Although the granites of the Vinquis batholith were assumed Ordovician (e.g., Grosse et al., 2011), we show that the granites were emplaced in the Early Carboniferous close to the Devonian-Carboniferous boundary.

3. Analytical methods

Numerous samples were collected mainly from the eastern, northern and southern flanks of the Vinquis batholith along the full length of ~51 km. Sixteen samples were selected for petrographic investigation. Based on these results and our numerous field observations, we chose representative samples: four for complete determination of mineral, nine for whole-rock chemistry including major and trace elements, three for Sm-Nd whole-rock isotope analyses and one for U–Pb and Lu-Hf isotope analyses of magmatic zircon. Location of samples is shown in Fig. 2.

Analytical methods for the determination of mineral and whole-rock chemistry, whole-rock Sm-Nd isotopes, and U–Pb and Hf isotopes from magmatic zircon are reported in Dahlquist et al. (2014, 2016) and in electronic Appendix A. Full data of U–Pb age are given in electronic Appendix C.

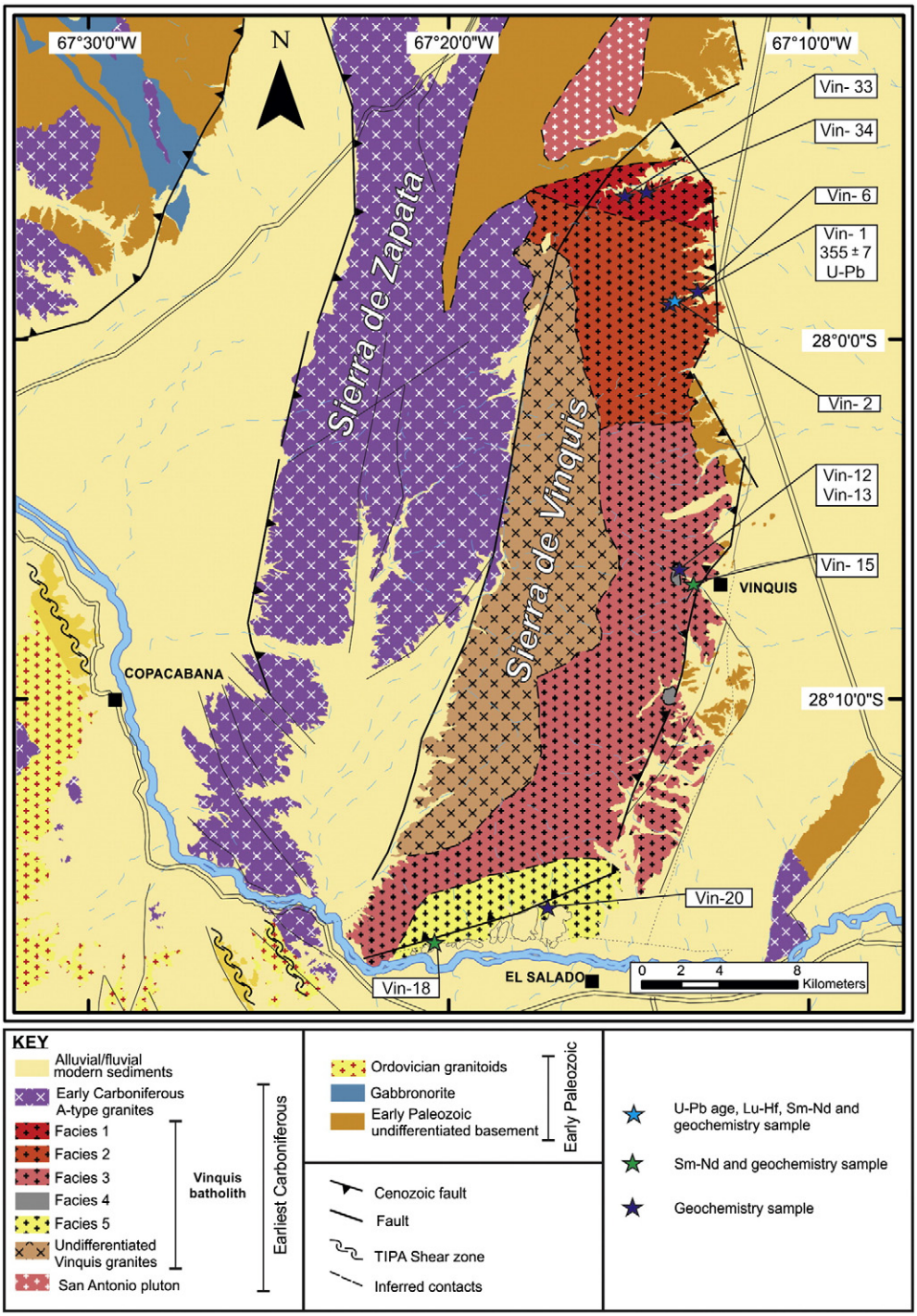

Fig. 2. Simplified geological map of Vinquis batholith showing the granitic facies recognized in the present work. Samples with whole-rock and mineral chemistry, and isotopic data are shown in the figure.
(Modified from Gonzalez Bonorino, 1972; Sosic, 1972; Höckenreiner et al., 2003; Toselli et al., 2014.)

4. Petrological characteristics of the Vinquis batholith

Many Early Carboniferous granites in the Sierras Pampeanas show subcircular forms (e.g., Los Arboles pluton, San Blas pluton, Capilla del Monte pluton, see Dahlquist et al., 2010a, Dahlquist et al., 2016). However, the Vinquis batholith is an elongate body with a major axis of ~43 km long in a northeastern-direction. On the western flank of the Sierra de Vinquis a major fault separates it from the Sierra de Zapata, which is formed by metaluminous A-type granites with an age of 340 Ma (Dahlquist et al., 2010a; Dahlquist et al., 2013). Toselli et al. (1992) divided the granites on either side of this fault, although more field-work is required to confirm this. Therefore, the granites of western flank appear in Fig. 2 as undifferentiated, and the relation between eastern and western facies remains unknown.

4.1. Host rocks

Metamorphic and mylonitic rocks are scarce (Fig. 2) and they are mostly observed as small scattered inliers in the recent sediments of the eastern flank (Lazarte, 2013; Sosic, 1972; Toselli et al., 1992). A larger outcrop (outside the study area) is located in the northern end of the Vinquis batholith (Fig. 2). These rocks were described by Lazarte (2013) as fine- to very fine-grained biotite schists and quartz-biotite phyllites. They show penetrative foliation (N305°/70°SW), and in some places a contact metamorphic overprint evident, leading to the formation of hornfels. Small scattered outcrops of mylonitic and protomylonitic rocks derived granitic protoliths as well as gneiss and migmatites were observed in the eastern flank. The mylonitic bands are clearly truncated by the Vinquis granites (Larrovere et al., 2016; Miller and Söllner, 2005). Gneisses and migmatites of centimeric grain-size occurring as xenoliths in the granite are of unknown age.

4.2. Granites

4.2.1. Petrographic data

The eastern flank of Vinquis batholith is largely dominated by two-mica monzogranites. The magmatic mineral assemblage is Qz + Afs + Pl + Bt + Ms with Ap + Zrn + Mnz ± Ilm as accessories (mineral abbreviations from Whitney and Evans, 2010). Oxides are scarce, erratically distributed, and only observed in some thin sections.

On the basis of textural and mineral studies, five dominant lithologies or facies are recognized in the eastern flank of the Vinquis batholith. Their distribution from north to south is (Fig. 2): *Facies 1*: white medium-grained porphyritic biotite-muscovite monzogranite, with poikilitic microcline phenocrysts (1–4 cm) enclosed in a medium equigranular matrix (1–4 mm); *Facies 2:* medium-grained equigranular two-mica monzogranite (1–5 mm), generally leucocratic, with the occasional or erratic presence of garnet phenocrysts (1–3 mm); *Facies 3*: coarse- to medium-grained porphyritic biotite-muscovite monzogranite with Afs phenocrysts (2–5 cm) in an equigranular matrix with variable grain-size (2–8 mm); *Facies 4:* gray fine-grained leucocratic two-mica equigranular monzogranite occurring as minor intrusive bodies within the porphyritic granite; *Facies 5*: coarse- to medium-grained (2–8 mm) leucocratic inequigranular pink monzogranite with isolated Afs phenocrysts, muscovite > biotite and occasional tourmaline and sillimanite (modal data are found in electronic Appendix B). Facies 3 is the dominant facies in the Vinquis batholith (Fig. 2) and the observed contacts with facies 4 and 5 are sharp. Similar sharp contacts for granitic facies emplaced synchronously have been reported by Dahlquist et al. (2007).

Centimetrics to metrics enclaves of fine-grained granitic composition with Afs phenocrysts are common in the Vinquis granites (mainly in Facies 1 and Facies 3). Pegmatites (~70 cm wide) with the assemblage Qz + Afs + Pl + Ms + Bt and Tur, Ap, Grt, Brl and Hem as accessory minerals, were recognized. Tungsten ore occurring as wolframite-bearing quartz veins or pegmatites emplaced in the porphyritic granite (Facies 5) was reported by Ávila et al. (1999).

4.2.2. Mineral composition

The results of complete electron microprobe analyses of plagioclase and K-feldspar are listed in Tables 1 and 2. Representative K-

Table 2
Representative composition of alkali feldspar in granites in Vinquis batholith from electron microprobe.

Facies	2	5	1
Sample	Vin-6	Vin-20	Vin-34
	Afs	Afs	Afs
Analysis number	Average $n = 5$	Average $n = 3$	Average $n = 6$
wt.%			
SiO_2	64.62	64.21	63.99
Al_2O_3	19.03	19.11	18.98
CaO	0.02	0.01	0.02
Na_2O	1.20	1.23	0.83
K_2O	14.69	14.66	15.31
P_2O_5	0.26	0.38	0.34
Total	99.83	99.60	99.46
% molar			
Ab	11.1	11.3	7.7
An	0.1	0.1	0.1
Or	88.9	88.7	92.2

Table 1
Representative composition of plagioclase in granites in Vinquis batholith from electron microprobe.

Facies	2				5	1			
Sample	Vin-6				Vin-20	Vin-34			
	Pl a		Pl b		Pl	Pl a		Pl b	
Analysis number	Pl 5 core	Pl 3 rim	Pl 19 rim	Pl 21 core	Average $n = 7$	Pl 16 core	Pl 22 rim	Pl 26 core	Pl 28 rim
wt.%									
SiO_2	65.16	66.21	68.17	66.51	64.59	62.38	66.07	64.98	67.71
Al_2O_3	21.59	20.98	20.37	21.18	22.54	23.67	21.85	21.89	20.44
CaO	2.07	1.51	0.62	1.65	2.72	4.44	1.80	2.22	0.58
Na_2O	10.33	10.70	11.54	10.95	9.48	8.75	10.08	9.88	10.95
K_2O	0.25	0.18	0.18	0.19	0.38	0.20	0.13	0.16	0.13
P_2O_5	0.28	0.04	0.19	0.30	0.24	0.18	0.38	0.27	0.07
Total	99.69	99.61	101.07	100.79	99.95	99.62	100.32	99.40	99.88
% molar									
Ab	88.7	91.9	96.2	91.3	84.4	77.2	90.3	88.1	96.4
An	9.8	7.1	2.9	7.6	13.3	21.6	8.9	10.9	2.8
Or	1.4	1.0	1.0	1.0	2.2	1.2	0.7	1.0	0.7

Table 3
Representative composition of biotite in granites in Vinquis batholith from electron microprobe.

Facies	2	5	1
Sample	VIN-6	VIN-20	VIN-34
	Bt	Bt	Bt
Analysis number	Average $n = 4$	Average $n = 4$	Average $n = 4$
wt.%			
SiO_2	36.25	35.37	35.87
TiO_2	2.39	2.32	2.91
Al_2O_3	19.48	19.74	18.75
Cr_2O_3	0.02	bdl	bdl
FeO	21.31	23.49	21.75
MnO	0.56	0.94	0.58
MgO	6.50	4.94	7.23
ZnO	0.11	bdl	bdl
CaO	bdl	bdl	bdl
Na_2O	0.09	0.13	0.11
K_2O	9.36	9.26	9.40
F	1.29	1.27	0.85
Cl	0.01	0.09	0.05
Total	97.38	97.61	97.58
O_F_Cl	0.55	0.56	0.37
CTotal	96.84	97.06	97.22
^{IV}Al	2.74	2.81	2.80
$[Fe^{2+}/(Fe^{2+} + Mg)]$	0.65	0.73	0.63

feldspar compositions range from Or_{89} to Or_{92}; those of plagioclase from An_{22} to An_3.

The biotite of the Vinquis granites has high siderophyllite–eastonite contents with $Fe^{2+}/(Fe^{2+} + Mg)$ ranging from 0.61 to 0.74 and Al^{IV} from 2.66 to 2.83 a.p.f.u. (Table 3). It also has high and distinctive F contents (average F = 1.17%, Table 3) similar to those of biotite in the Early Carboniferous A-type granites and Late Devonian strongly peraluminous A-type granites of the Sierras Pampeanas (Dahlquist et al., 2010a; Dahlquist et al., 2014; Dorais et al., 1997).

White mica is the other sheet silicate present in the Vinquis batholith. Petrographic observations using the criteria of Miller et al. (1981) suggest that both primary and secondary muscovite types are present. Complete electron microprobe analyses for the muscovite are listed in Table 4. Muscovite occurring as subhedral to euhedral medium-grained unaltered single crystals, is assumed to be primary; its chemical composition falls in the appropriate field of the Mg–Ti–Na diagram (figure not shown) according to the subdivision of Miller et al. (1981), similar to magmatic muscovite coexisting with aluminous minerals (e.g., Alasino et al., 2010; Clarke et al., 2005; Dahlquist et al., 2005, 2007 and references therein). Thus, both textural and chemical evidence indicates a primary origin for some of the muscovite of the Vinquis batholith.

Table 4
Representative composition of muscovite in granites in Vinquis batholith from electron microprobe.

Facies	2	5	1
Sample	VIN-6	VIN-20	VIN-34
	Ms	Ms	Ms
Analysis number	Average $n = 4$	Average $n = 4$	Average $n = 2$
wt.%			
SiO_2	46.01	45.95	46.23
TiO_2	0.87	0.66	0.85
Al_2O_3	34.03	34.02	34.45
Cr_2O_3	0.00	0.00	0.00
FeO	2.00	2.85	1.98
MnO	0.03	0.07	0.03
MgO	0.84	0.76	0.78
ZnO	0.02	bdl	bdl
CaO	bdl	bdl	bdl
Na_2O	0.49	0.56	0.49
K_2O	10.28	10.33	10.34
F	0.49	0.72	0.29
Cl	bdl	bdl	bdl
Total	95.07	95.96	95.51
O_F_Cl	0.21	0.31	0.12
CTotal	94.86	95.66	95.39

Table 5
Representative composition of apatite in granites in Vinquis batholith from electron microprobe.

Facies	2	5	1
Sample	VIN-2	VIN-20	VIN-34
	Ap	Ap	Ap
Analysis number	Average $n = 2$	Average $n = 2$	Average $n = 2$
wt.%			
P_2O_5	40.34	38.92	39.89
FeO	0.72	0.38	0.21
MnO	3.15	2.39	0.54
MgO	0.04	0.02	0.04
CaO	51.84	52.24	54.07
Na_2O	0.08	0.15	0.06
K_2O	0.01	bdl	bdl
F	3.59	4.68	4.83
Cl	0.04	0.06	0.01
Y_2O_3	bdl	0.32	0.18
Total	99.80	99.15	99.81

bdl = below detection limit.

The apatite is fluorapatite (F = 4.9% to 3.31%, Table 5). Systematic electron-microprobe analysis in thin sections (including Zr and LREE data) indicates the presence of two radioactive minerals, zircon and monazite, and the presence of two oxides, ilmenite and rutile.

Phenocrysts of garnet form roughly hexagonal euhedral to subhedral sections, with diameters between 1 and 3 mm and few or no

Table 6
Representative composition of garnet in granites in Facies 2 of Vinquis batholith from electron microprobe.

Sample	VIN-2 (Facies 2)			
Mineral	Grt central area	Grt central area	Grt margin area	Grt margin area
Analysis location	42	37	35	34
	Circle 16			
wt.%				
SiO_2	36.11	35.64	36.05	35.89
TiO2	bdl	bdl	bdl	bdl
Al_2O_3	21.88	21.96	21.88	21.90
FeO	25.36	25.47	27.27	26.78
MnO	17.83	17.19	14.97	15.86
MgO	0.73	0.78	0.92	0.92
CaO	0.36	0.33	0.30	0.29
Na_2O	bdl	bdl	bdl	bdl
Total	102.27	101.36	101.39	101.62
End-members calculated following Deer et al. (1992)				
Pyrope	2.865	3.092	3.696	3.638
Almandine	56.131	57.001	61.333	59.722
Spessartine	39.974	38.971	34.107	35.826
Grossular	1.03	0.935	0.864	0.814
Andradite	0	0	0	0
Alm + Sps	96.105	95.972	95.44	95.548

In those cases where the Total is low the total iron is expressed as ferric iron.
Bdl: below detection limit.

Table 7
Major element (in %) and trace element (in ppm) concentrations of the Vinquis granites.

Rock	Facies 1	Facies 2	Facies 2	Facies 3	Facies 3	Facies 4	Facies 5	Facies 5	Felsic enclave in Facies 1
Latitude (S)	27°55′46.1″	27°58′44.9″	27°58′47.2″	28°06′29.7″	28°06′39.3″	28°06′29.7″	28°16′44.0″	28°15′43.9″	27°55′38.9″
Longitude (W)	67°15′04.7″	67°13′53.3″	67°13′32.2″	67°13′44.7″	67°13′12.1″	67°13′44.7″	67°20′19.6″	67°17′22.2″	67°14′31.7″
Samples	VIN-33	VIN-1	VIN-5	VIN-13	VIN-15	VIN-12	VIN-18	VIN-20	VIN-34
Element									
SiO_2	71.52	72.46	72.92	71.60	72.59	72.37	73.97	74.83	72.10
TiO_2	0.31	0.19	0.19	0.43	0.25	0.29	0.16	0.10	0.28
Al_2O_3	14.74	14.53	14.67	13.98	14.75	14.29	14.02	14.09	14.75
FeO*	2.20	1.31	1.31	2.36	1.56	1.87	1.29	0.76	1.89
MnO	0.04	0.05	0.05	0.05	0.04	0.03	0.07	0.02	0.04
MgO	0.69	0.37	0.33	0.71	0.46	0.49	0.23	0.13	0.58
CaO	0.84	0.73	0.69	1.40	0.73	0.86	0.66	0.54	0.82
Na_2O	2.99	3.15	3.46	3.10	3.08	2.60	3.13	3.09	3.06
K_2O	5.15	5.03	4.85	4.55	5.42	5.82	4.76	5.26	5.13
P_2O_5	0.29	0.34	0.36	0.31	0.31	0.37	0.33	0.23	0.32
LOI	0.84	0.92	0.91	0.96	0.89	1.02	0.85	0.91	0.80
TOTAL	98.78	98.17	98.82	98.50	99.17	98.99	98.61	99.04	98.97
X_{Fe}	0.76	0.78	0.80	0.77	0.77	0.79	0.85	0.85	0.77
$K_2O + Na_2O$	8.15	8.18	8.31	7.65	8.49	8.42	7.89	8.35	8.19
K_2O/Na_2O	1.72	1.60	1.40	1.47	1.76	2.24	1.52	1.70	1.68
ASI^{I}	1.23	1.22	1.20	1.11	1.20	1.18	1.22	1.20	1.22
ASI^{II}	1.30	1.30	1.29	1.18	1.28	1.27	1.31	1.26	1.30
AI	0.71	0.73	0.75	0.72	0.74	0.74	0.73	0.77	0.72
ppm									
Cs	15.42	20.56	13.60	5.88	17.10	6.87	27.63	30.30	18.09
Rb	338.99	387.70	407.41	282.32	350.45	320.88	447.24	327.40	343.88
Sr	70.08	45.81	36.91	116.25	61.19	70.48	26.83	29.17	67.62
Ba	321.61	160.32	135.87	355.71	242.10	272.58	82.00	50.47	275.22
La	35.09	16.90	16.23	46.87	22.03	30.27	13.41	6.83	29.62
Ce	74.73	37.79	36.47	103.11	48.65	68.16	29.87	15.28	64.68
Pr	8.95	4.66	4.48	12.41	5.98	8.35	3.65	1.91	7.82
Nd	32.76	17.33	16.67	46.61	22.28	30.88	13.46	7.06	28.99
Sm	7.31	4.37	4.12	9.39	5.13	7.44	3.43	1.79	6.96
Eu	0.87	0.50	0.44	1.13	0.69	0.74	0.38	0.28	0.78
Gd	5.59	3.77	3.44	6.74	4.05	6.14	3.19	1.63	5.39
Tb	0.80	0.64	0.60	0.97	0.62	1.02	0.63	0.31	0.84
Dy	3.93	3.36	2.92	5.00	3.21	5.42	3.77	1.91	4.06
Ho	0.63	0.52	0.47	0.90	0.55	0.92	0.68	0.36	0.64
Er	1.48	1.17	1.07	2.20	1.35	2.15	1.83	1.00	1.51
Tm	0.20	0.15	0.15	0.28	0.19	0.29	0.28	0.15	0.20
Yb	1.19	0.82	0.89	1.62	1.12	1.74	1.76	0.95	1.20
Lu	0.17	0.11	0.12	0.24	0.17	0.25	0.26	0.14	0.17
U	4.75	3.27	2.88	4.33	2.57	4.31	6.60	4.47	4.25
Th	19.71	11.28	11.00	31.79	14.14	20.73	9.58	6.07	17.51
Y	17.15	14.59	12.99	23.02	14.92	25.05	19.60	10.79	17.83
Nb	18.22	16.85	24.02	21.55	16.35	19.95	26.01	11.53	17.88
Zr	140.96	86.70	81.01	180.63	105.07	145.54	70.58	37.24	132.05
Hf	4.24	2.79	2.63	5.11	3.13	4.32	2.43	1.45	3.98
Ta	2.08	3.54	3.41	2.48	2.07	1.61	4.02	2.16	2.60
Ni	3.50	4.23	3.12	4.40	4.74	3.02	2.32	0.81	2.40
Cr	12.20	7.26	6.35	7.20	9.17	7.16	6.45	5.44	10.00
Sc	4.46	3.02	3.83	5.40	4.64	3.73	5.04	2.82	4.25
V	28.50	14.82	12.50	36.20	26.11	20.36	12.00	8.77	23.80
Ga	22.10	21.97	22.68	20.90	21.47	19.86	23.99	19.35	22.90
Cu	1.60	2.32	9.37	3.60	2.92	1.21	1.51	6.85	5.20
Zn	78.90	60.38	65.62	67.70	63.30	62.19	46.57	28.63	73.20
Pb	31.20	28.83	25.10	27.40	30.95	34.27	23.49	28.63	30.30
Al	78,011	76,900	77,641	73,989	78,064	75,630	74,201	74,571	78,064
ΣREE	174	92	88	237	116	164	77	40	153
$(La/Yb)_N$	19.64	13.77	12.18	19.31	13.13	11.61	5.09	4.81	16.45
$(Eu/Eu^*)_N$	0.42	0.38	0.36	0.44	0.47	0.34	0.36	0.51	0.39
10,000× Ga/Al	2.83	2.86	2.92	2.82	2.75	2.63	3.23	2.59	2.93
Zr + Nb + Ce + Y	251.07	155.94	154.49	328.32	184.99	258.69	146.06	74.84	232.44
M	1.20	1.19	1.21	1.32	1.22	1.24	1.17	1.18	1.20
T_{Zr}	789	749	743	803	763	790	735	685	784

Explanation: Total iron as FeO; major element oxides in wt.%, trace elements in ppm. XFe = FeO/(FeO + MgO). TZr (°C) was calculated following Miller et al. (2003) and Dahlquist et al. (2010a). Geothermometer was calibrated for M = 0.9 to 1.7. All granitic rocks are monzogranites according to the G1-G2-G3 + G4 multicationic classification (homologous to the modal classification of Streckeisen, 1976) of de La Roche (1992). ASI^{I} by Shand (1927) = $Al_2O_3/[(CaO + Na_2O + K_2O]$ (mol.). ASI^{II} by Zen (1986) = All ASI values calculated using CaO_{corr}. CaO_{corr} = All CaO values assuming all P_2O_5 is in apatite, CaO_{corr} = CaO (% mol.) − 3.33 × P_2O_5 (% mol.).

apatite inclusions. The garnet is largely a solid solution of almandine and spessartine, which constitutes 95–96% of the total composition (Table 6): pyrope and grossular together make up the remainder. Both textural and chemical data indicate a primary origin for the garnet as was largely discussed by Dahlquist et al. (2007 and references therein).

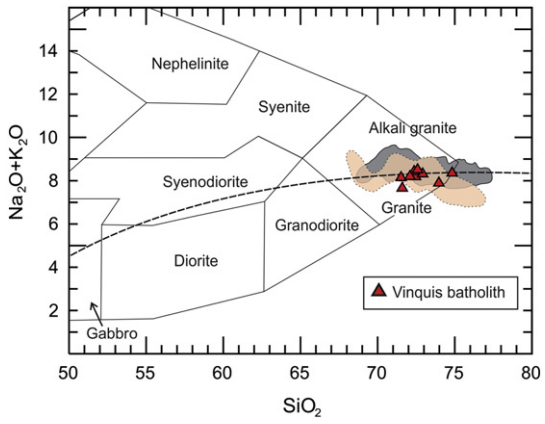

Fig. 3. SiO_2 vs. $Na_2O + K_2O$, wt.% variation diagram for the Vinquis batholith granitic samples. The gray and pale orange fields represent Early Carboniferous metaluminous to weakly peraluminous A-type granites and strongly peraluminous A-type Late Devonian and Early Carboniferous granitic samples in the Sierras Pampeanas, respectively. The alkaline/subalkaline curve is after Miyashiro (1978).
(Data from Dahlquist et al., 2010a; Dahlquist et al., 2010b, 2014, 2016.)

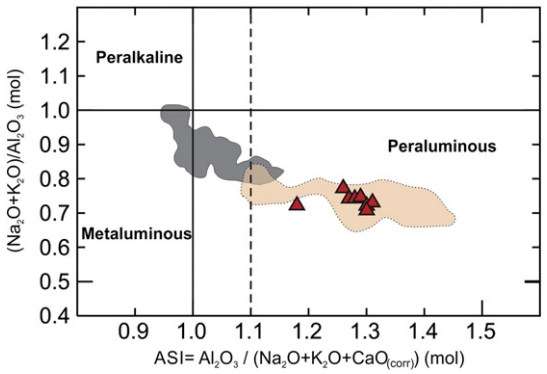

Fig. 5. Alumina saturation index (ASI) in the studied granitic rocks. The samples range in ASI (using the formulation of Zen (1986) = 1.18–1.31, with relatively low values for the ASI index. Boundary ASI = 1 from Shand (1927), ASI = 1.1 from Chappell and White (1992). The gray and pale orange fields are those showed in Fig. 3.

5. Whole-rock compositions

5.1. Major elements

All the granitic rocks of Vinquis batholith are monzogranites with SiO_2 contents in a restricted range from 71.5% to 74.8% (Table 7). In the alkalis vs. silica classification diagram of Wilson (1989), they plot at the silica-rich end close to the limit between alkali and subalkaline granitic field. They also plot mainly within the field of Carboniferous metaluminous to weakly peraluminous A-type granites in the Sierras Pampeanas (Fig. 3).

These monzogranites are poor in Ca (0.54–1.4% CaO) and rich in FeO^t, with high $FeO^t/(FeO^t + MgO)$ values ranging from 0.77 to 0.86 (average = 0.80), where the southern facies shows the highest values (Table 7). They are also enriched in MgO relative to Ti (MgO/TiO_2> 1.2) and moderately enriched in total alkalis (8.18 wt% average), with high K_2O contents relative to Na_2O (K_2O/Na_2O = 1.40–2.24). As with other peraluminous A-type granites in the Sierras Pampeanas and worldwide, these granitic rocks follow the alkali-calcic trends in the Na_2O+K_2O–CaO vs. SiO_2 diagrams of Frost et al. (2001) (Fig. 4a). In the $FeO^t/(FeO^t+MgO)$ vs. SiO_2 diagrams of Frost et al. (2001) the most samples plot in the magnesian field although near to the magnesian – ferroan boundary (Fig. 4b).

The Vinquis granites are strongly peraluminous, with ASI (molar ratio of $(Al_2O_3/[CaO + Na_2O + K_2O])$ according to Shand, 1927) ranging from 1.11 to 1.23. The calculated ASI using the formulation of Zen (1986) is slightly higher (ASI = 1.18–1.31) because the P_2O_5 content is combined with the CaO (Fig. 5). Both values are included in Table 7. The high P_2O_5 content (0.23–0.37%) is a distinctive feature, close to values recently reported for Paleozoic F-rich peraluminous A-type granites in the Sierras Pampeanas (e.g., the Achala batholith and Capilla del Monte pluton in the Sierras de Córdoba and the El Pilón stock in Sierra Brava, Dahlquist et al., 2010b, 2014, 2016).

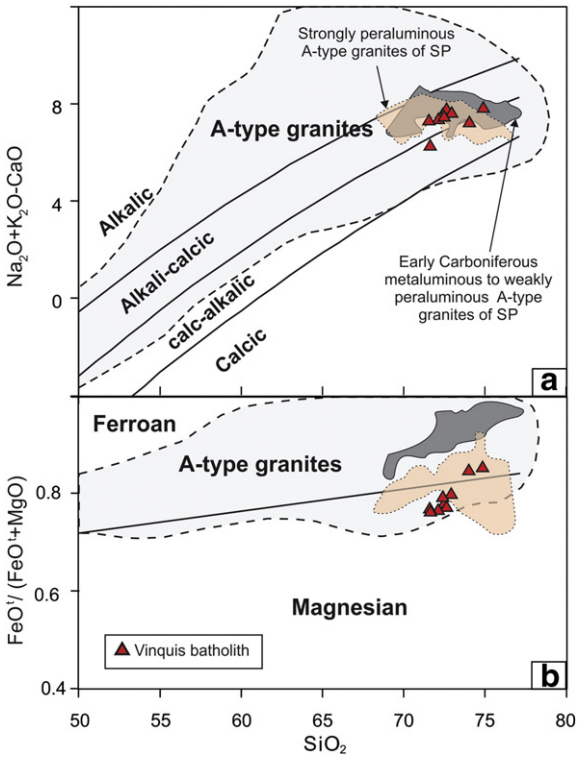

Fig. 4. Studied granites plotted on the classification diagrams of Frost et al. (2001): (a) $Na_2O + K_2O - CaO$ vs. SiO_2, wt.% and (b) $FeO^t/(FeO^t + MgO)$ vs. SiO_2, wt.%. The A-type granite field is after Frost et al. (2001). Abbreviation: SP = Sierras Pampeanas.

5.2. Trace elements and REE

The granites of the Vinquis batholith have low to medium abundance of rare-earth elements (REE, 40–237 ppm). All granitic facies show significant negative Eu anomalies (Eu/Eu^* = 0.34–0.51). Two distinctive chondrite-normalized REE patterns are observed (Fig. 6a). The granitic facies of the central and northern region show a relative increase of LREE with respect to the southern facies ($[La/Yb]_N$ = 11.6–19.6 and 4.8–5.1, respectively).

Primitive-mantle normalized spider diagrams show marked negative Ba, Nb, Sr, Eu and Ti anomalies and significant enrichment in Cs, Rb, and moderate enrichment of Th, U (Fig. 6b). The P content is higher when is compared with that reported for Carboniferous metaluminous A-type granites of the Sierras Pampeanas (Fig. 6b). Fig. 7 shows the trends defined by some trace elements as a function of mafic content. The Vinquis granites show well-defined positive correlations of Th, LREE, Zr and Hf contents with FeO^t + MgO (see Section 7.3).

The Vinquis granites are characterized by high Ga/Al values, with 10,000 × Ga/Al values ranging from 2.59 to 3.23 (Table 7). These values are similar to other typical A-type granites with values >2.6 (Whalen et al., 1987). The granites have medium to low contents of high field-

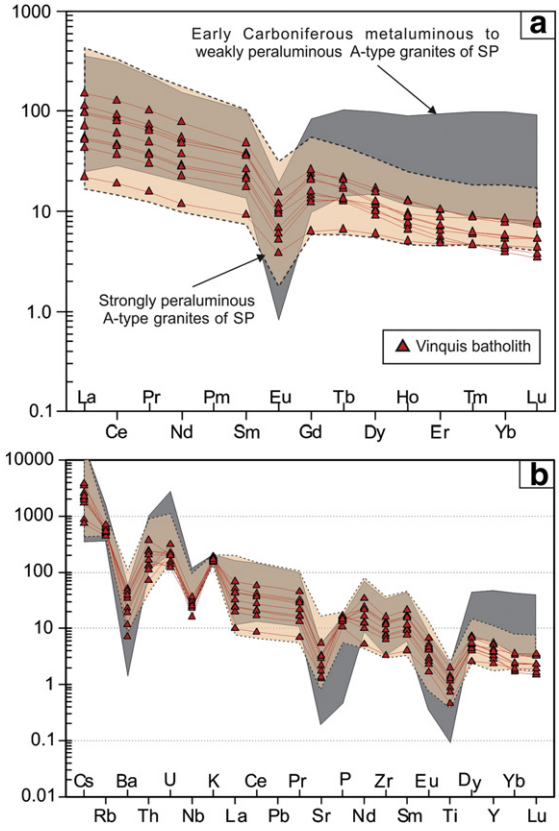

Fig. 6. (a) Chondrite-normalized (Boynton, 1984) REE plots for granites of the Vinquis batholith. The granite rocks of the Vinquis batholith have REE patterns similar to those reported for metaluminous to weakly peraluminous Carboniferous A-type granites (Dahlquist et al., 2010a) although the former are impoverished in HREE. REE patterns of the strongly peraluminous Paleozoic A-type granite of Sierras Pampeanas (Dahlquist et al., 2014, 2016) are similar to those REE pattern for the granites of the Vinquis batholith. (b) Primitive mantle-normalized (Sun and McDonough, 1989) spider diagrams. The granitic rocks of the Vinquis batholith and strongly peraluminous Paleozoic A-type granites have similar compositions to those reported for Carboniferous metaluminous to weakly peraluminous A-type granites of the Sierras Pampeanas (see Dahlquist et al., 2010a), although the former are significantly enriched in P.

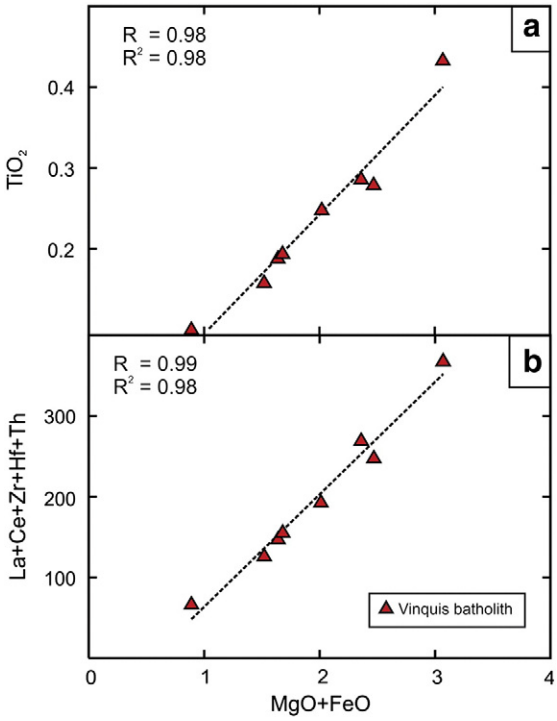

Fig. 7. Whole-rock TiO_2 vs (FeO^t + MgO), (a) and La + Ce + Zr + Hf + Th vs. FeO^t + MgO, (b) for eight granite samples for the Vinquis batholith. Regression lines are projected in the figures.

strength elements (HFSE) such as Zr (37–181 ppm), Y (11–25 ppm), Nb (12–26) and Ce (15–103). Total Zr + Nb + Ce + Y contents range from 75 to 328 ppm – lower than reported for typical A-type granites (>350 ppm, Whalen et al., 1987) and also lower than those reported by Dahlquist et al. (2010a) for Early Carboniferous metaluminous to weakly peraluminous A-type granites of the Sierras Pampeanas (average, Zr + Nb + Ce + Y = 414 ppm).

6. Geochronological and isotopic data for the Vinquis batholith

6.1. U–Pb LA-MC-ICP-MS zircon age

The combined SEM-CL and optical images reveal that the zircon grains separated from VIN-1 (Facies 2 of Vinquis batholith) are mostly elongate prismatic with oscillatory zoning and subhedral to euhedral terminations, in some cases developed over a distinct core (Fig. 8a and Table 8).

One group of analyses, mostly located in the outer oscillatory zoning, gave consistent $^{206}Pb/^{238}U$ ages varying from 334 Ma to 369 Ma (see Table 8). Nine data points yield a Tera-Wasserburg Concordia age (Ludwig, 2003) of 355 ± 7 Ma (2σ confidence limits, allowing for the uncertainty in U/Pb calibration), which is considered the best estimate for the crystallization of the host monzogranite (Fig. 8b). This age essentially overlaps the Devonian–Carboniferous boundary (358.9 ± 0.4 Ma, IUGS stratigraphic chart, 2015, http://www.stratigraphy.org/index.php/ics-chart-timescale). Other analyses, mostly located in the core zones, reveal inherited zircon ages concentrated at Cambrian (n = 4) and Ordovician (n = 5) times (Fig. 8a). One grain yielded a Mesoproterozoic inheritance zircon age.

6.2. Hf isotope data

The magmatic zircon has variable $\varepsilon_{Hf,t}$ values (t = 355 Ma, time of crystallization), ranging from −9.5 to −1.5, although mostly in the range −6.8 to −4.9 (Table 9 and Fig. 9); and there is a Mesoproterozoic average T_{DM} of 1.69 Ga (Table 9).

The inherited Cambrian and Ordovician zircon has negative $\varepsilon_{Hf,t}$ (ranging from −1.2 to −5.7 at time of crystallization) with a similar average T_{DM} (1.56 Ga; Table 9). Notably, at the time the granite crystallized (t = 355 Ma), $\varepsilon_{Hf,t}$ values from the inherited zircons would have been comparable to those of the zircons that crystallized at that time ($\varepsilon_{Hf,t}$ = −4.1 to −6.7).

6.3. Sm-Nd isotope data

Three samples from the Vinquis batholith were analyzed for their Nd isotopic composition. All samples have roughly similar $^{147}Sm/^{144}Nd$ (0.135–0.153) and $^{143}Nd/^{144}Nd$ (0.51212–0.51222) ratios. Epsilon Nd values (ε_{Ndt}) calculated to 355 Ma (Table 10) are strongly negative, ranging from −6.1 to −7.8 (average = −7.1). The Nd model ages were calculated through a two-stage model following De Paolo et al. (1991), which is appropriate for granitic rocks derived by the partial melting of old continental lithosphere characterized by high $^{147}Sm/^{144}Nd$ ratios (Milisenda et al., 1994). The T_{DM} are between 1.59 Ga and 1.71 Ga, i.e., Mesoproterozoic (Table 10).

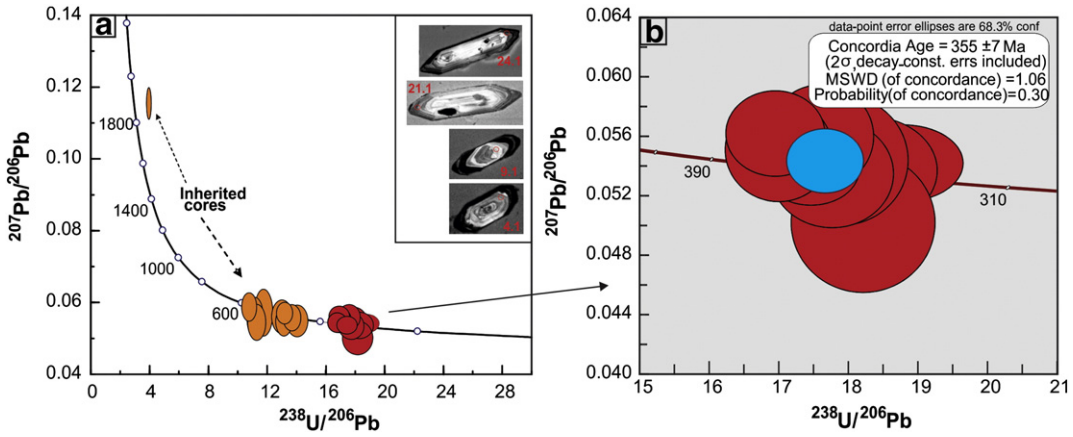

Fig. 8. U–Pb LA-MC-ICP-MS zircon dating of sample VIN-1 (Facies 2) from the northeastern of the Vinquis batholith, (a). Inherited core zircon ages are also shown (orange color). The main Tera-Wasserburg plot shows most analyses plotting between 334 and 369 Ma, and the *inset* shows a Concordia age calculation of 355 ± 7 Ma, (b). Selected zircon images are also included. Data are reported in Table 8.

Table 8
LA-ICP-MS zircon U–Pb analytical results from VIN-1, of Vinquis batholith.

				Ratios				Ages (Ga)		
Grain	GCh SS	Spot	$^{238}U/^{206}Pb$	1 s	$^{207}Pb/^{206}Pb$	1 s	$^{206}Pb/^{238}U$	1 s	$^{207}Pb/^{206}Pb$	1 s
VIN-1	e,p,hd	23.1	18.7949	0.5667	0.0542	0.0017	0.334	0.01	0.38	0.072
VIN-1	e,p,hb	22.1	18.2964	0.6505	0.0537	0.0024	0.343	0.012	0.358	0.095
VIN-1	e,p,osc	21.1	18.2149	0.683	0.0502	0.0031	0.345	0.013	0.206	0.132
VIN-1	e,p,osc	24.1	17.8875	0.6431	0.0544	0.0029	0.351	0.012	0.387	0.127
VIN-1	c,p,osc	17.1	17.7698	0.5827	0.0535	0.0024	0.353	0.011	0.348	0.101
VIN-1	c,p,osc	2.1	17.6078	0.5004	0.056	0.0023	0.356	0.01	0.451	0.091
VIN-1	e,p,osc	3.1	17.4647	0.4592	0.0538	0.0016	0.359	0.009	0.362	0.066
VIN-1	c,p,hd	16.1	17.0023	0.5097	0.0551	0.0023	0.368	0.011	0.418	0.091
VIN-1	e,p,osc	4.1	16.9517	0.4701	0.0562	0.0019	0.369	0.01	0.462	0.077
VIN-1 (inh-age)	m,p,osc	18.1	14.0772	0.4764	0.055	0.0029	0.442	0.015	0.414	0.119
VIN-1 (inh-age)	m,p,osc	6.1	13.71	0.3976	0.0558	0.0024	0.454	0.013	0.444	0.098
VIN-1 (inh-age)	c,p,osc	8.1	13.2159	0.3633	0.0571	0.002	0.47	0.012	0.495	0.077
VIN-1 (inh-age)	c,p,ic	12.1	13.1778	0.3771	0.0549	0.0027	0.472	0.013	0.409	0.11
VIN-1 (inh-age)	c,p,osc	14.1	13.0453	0.4687	0.0561	0.0031	0.476	0.017	0.456	0.124
VIN-1 (inh-age)	c,p,osc	1.1	11.7895	0.4166	0.0573	0.0043	0.525	0.018	0.503	0.153
VIN-1 (inh-age)	m,fr,hd	13.1	11.3205	0.4112	0.0546	0.0033	0.546	0.019	0.397	0.13
VIN-1 (inh-age)	c,p,hb	7.1	11.2199	0.3687	0.0559	0.0037	0.55	0.017	0.447	0.147
VIN-1 (inh-age)	e,p,osc	20.1	10.8045	0.3304	0.0588	0.0026	0.571	0.017	0.561	0.103
VIN-1 (inh-age)	c,p,osc	9.1	3.9714	0.0997	0.1153	0.0029	1.448	0.033	1.885	0.046

$^{238}U/^{206}Pb$ and $^{207}Pb/^{206}Pb$ ratios corrected for static fractionation using GJ 1.
Measurement errors represent within-run uncertainty only. All data points on magmatic zircons were used in calculated concordia age.
Grain characteristics (GCh) and site of the spot (SS): Site of the spot: e = end or edge. Habit of the grain: p = prism, fr = fragmented. CL images: osc = oscillatory zoning.
inh-age = inheritance age.
Location of sample is: 27° 58′ 44.9″–67° 13′ 53.3″.

Table 9
Laser ablation Hf isotope data for igneous dated zircons from sample VIN-1, Vinquis batholith.

Grain	Spot	$^{176}Hf/^{177}Hf$	±2 σ	$^{176}Lu/^{177}Hf$	±2 σ	U–Pb age (t) Ma	εHf (t)	T_{DM} (Ma)
VIN-1	2.1	0.282299	0.000058	0.001734	0.000093	355	−9.33	1894
VIN-1	3.1	0.282415	0.000065	0.001816	0.000074	355	−5.24	1637
VIN-1	4.1	0.282381	0.000048	0.002191	0.000083	355	−6.51	1717
VIN-1	16.1	0.282425	0.000027	0.001880	0.000105	355	−4.89	1614
VIN-1	17.1	0.282415	0.000049	0.003084	0.000131	355	−5.53	1655
VIN-1	21.1	0.282410	0.000024	0.001761	0.000006	355	−5.38	1646
VIN-1	22.1	0.282291	0.000055	0.001186	0.000090	355	−9.49	1904
VIN-1	23.1	0.282370	0.000031	0.001641	0.000033	355	−6.80	1735
VIN-1	24.1	0.282524	0.000077	0.002329	0.000050	355	−1.51	1401
VIN-1 (inh)	1.1	0.282443	0.000035	0.002036	0.000057	503	−1.23	1497
VIN-1 (inh)	8.1	0.282446	0.000044	0.003380	0.000046	495	−1.74	1523
VIN-1 (inh)	6.1	0.282452	0.000037	0.002649	0.000023	444	−2.33	1520
VIN-1 (inh)	14.1	0.282435	0.000029	0.001887	0.000007	456	−2.44	1537
VIN-1 (inh)	12.1	0.282376	0.000028	0.002242	0.000040	409	−5.66	1700

Laser operating conditions: GJ1 - 6 mJ ou 8.55 J/cm^2 (100%), 7 Hz, spot = 47 μm, He (MCF1) = 0.25 L/min, (MCF2) = 0.5 L/min, N2 = 1.2 mL/min, 50 ciclos, AR80 = 30 V.
t = crystallization age of the VIN-1, T = model age.
$^{176}Hf/^{177}Hf_{CHUR(t)} = 0.282548$.

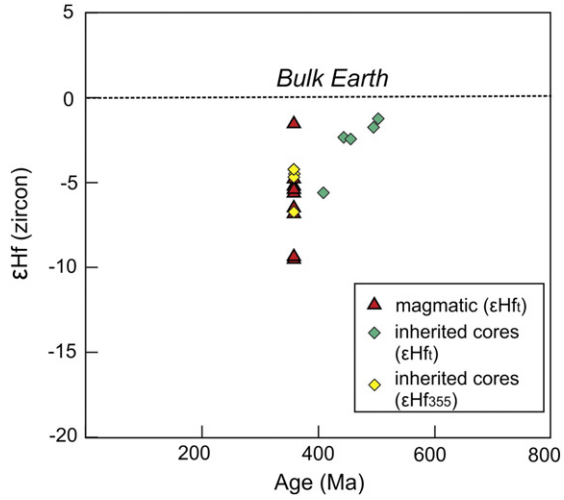

Fig. 9. Age versus εHft values for Early Carboniferous zircon hosted in VIN-1 granite, showing both measured and initial epsilon Hf values as function of crystallization age.

7. Discussion: genesis of the Vinquis batholith

7.1. Biotite chemistry as indicator of their parental magmas

Various studies (e.g., Abdel Rahman, 1994; Dahlquist et al., 2010a; Dahlquist et al., 2014, 2016; Shabani et al., 2003) demonstrate that the composition of igneous biotite reflects the nature of their parental magmas. In particular, Dahlquist et al. (2014) show that plots of FeO^t vs MgO and $Fe^{2+}/(Fe^{2+} + Mg)$ vs F may be useful to identify biotite in Paleozoic Sierras Pampeanas granites formed in different geodynamic settings. Biotite from the Vinquis batholith has a similar composition to that in the Late Devonian strongly peraluminous A-type granitic magmas (Fig. 10), but differs from that of biotite in the Early Carboniferous metaluminous to weakly peraluminous A-type granitic magmas. In general, biotite in the former, and in the Vinquis batholith, has relatively high FeO^t/MgO values (average from Vinquis granites = 3.34), but lower than in the Early Carboniferous biotite (average = 18.24), which also has relatively high and variable F content (Fig. 10a, b). The highest F content is observed in biotite in the strongly peraluminous A-type Late Devonian granites, the Vinquis batholith and some metaluminous Early Carboniferous A-type granites of Sierras Pampeanas (Fig. 10b).

Biotite from Ordovician strongly peraluminous granites (ASI ranging from 1.61 to 1.95, data from Dahlquist et al., 2005) in the Sierras Pampeanas, such as the Tuaní granite, is moderately enriched in Mg, with $FeO^t/MgO = 1.64$ and plots in the field of peraluminous biotite close to that of biotite from calc-alkaline granites (Fig. 10a). Biotite from both Ordovician metaluminous calc-alkaline and Tuaní granite has lower FeO^t/MgO and F contents than those of the Devonian/Carboniferous biotite (Fig. 10a, b).

Anderson and Morrison (2005) and Dall'Agnol and Oliveira (2007) have shown that the $Fe^{2+}/(Fe^{2+} + Mg)$ values of biotite are different for oxidized and reduced A-type granites, respectively. Three

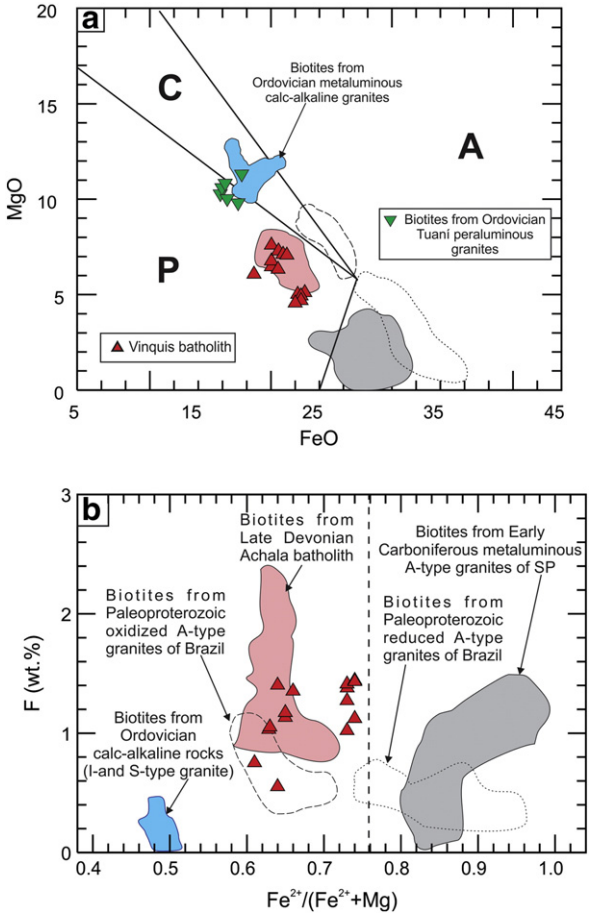

Fig. 10. Mineral composition for biotites crystallized from different granitic rocks (modified from Dahlquist et al., 2014). (a) FeO vs. MgO biotite discriminant diagram after Abdel Rahman (1994): biotite in anorogenic alkaline suites (A field), biotite in peraluminous granites (P field), and biotite in metaluminous calc-alkaline granite suites (C field). (b) $Fe^{2+}/(Fe^{2+} + Mg)$ vs. F wt.%. Dashed line represents a rough boundary for biotite crystallized from A-type granites in dominant reduced and oxidized conditions, respectively. The chemical data of biotite are from Dahlquist et al. (2010a), Dahlquist et al. (2014) and Dall'Agnol et al. (1999c, 2005). Abbreviation: SP = Sierras Pampeanas.

Paleoproterozoic A-type granitic suites that evolved in varying fO_2 conditions in the Carajás province of the eastern Amazonian craton (Brazil) were studied by Dall'Agnol et al. (2005) and Dall'Agnol and Oliveira (2007). Of these, the Jamon A-type granites crystallized in relatively oxidizing conditions and the biotite has $Fe^{2+}/(Fe^{2+} + Mg)$ ratios between 0.6 to 0.7, close to the values observed in the biotite of the Vinquis batholith (0.63–0.73). Conversely, biotite from the Velho Guilherme and Serra dos Carajás suites that evolved under reducing conditions has higher $Fe^{2+}/(Fe^{2+} + Mg)$ ratios ranging from 0.75 to 0.95, similar to the of biotite from metaluminous to weakly peraluminous A-type granites in the Sierras Pampeanas (0.81 to 0.98, Fig. 10b).

Table 10
Sm–Nd isotopic compositions for the granites of the Vinquis batholith.

Sample	Rock type	Sm ppm	Nd ppm	$^{147}Sm/^{144}Nd$	$^{143}Nd/^{144}Nd$	$(^{143}Nd/^{144}Nd)t$	εNdt	T_{DM}^* (Ga)
VIN-1	EG, Facies 2	2.524	10.431	0.1463	0.512121	0.511778	−7.81	1.71
VIN-15	PG, Facies 3	3.296	14.711	0.1354	0.512117	0.511800	−7.39	1.68
VIN-18	PG, Facies 3	1.809	7.14	0.1532	0.512224	0.511865	−6.11	1.59

PG = porphyritic granite, EG = equigranular granite.
t = 355 Ma, T_{DM}^* after De Paolo et al. (1991).

It is important to note that biotite which crystallized from strongly peraluminous magmas (orogenic or S-type granites) can have similar FeO^t/MgO values and Al^{IV} content (e.g., Abdel Rahman, 1994; Clarke et al., 2005; Dahlquist et al., 2005, 2007 and references therein) to that of biotite in strongly peraluminous A-type granites. Therefore, biotite compositions should be interpreted in combination with other data (e.g., whole-rock compositions). The biotite compositions reported here are strongly consistent with the whole-rock chemistry discussed in Section 7.4.

7.2. Geochronological constraints and source of the granitic magmas

The geochronological data reported in Section 6 indicate that the granites of the Vinquis batholith were emplaced at 355 ± 7 Ma, overlapping the Devonian-Carboniferous boundary (t = 358.9 Ma). This new data and our previous geochronological data (see Section 2) indicate that metaluminous and peraluminous A-type plutons were mainly emplaced synchronously in the foreland region.

Inherited zircon ages reported above show major Early Ordovician and Early Cambrian composite peaks, which correspond to the previous magmatic episodes of the Famatinian and Pampean orogenies (Fig. 8a). These data strongly suggests a dominant local metasedimentary protolith (from a constrained basin receiving weathered material from Pampean and Famatinian rocks) for the Vinquis granites. The Vinquis granites have marked negative $\varepsilon_{Nd,t}$ (−6.1 to −7.8) and zircon $\varepsilon_{Hf,t}$ values (−9.5 to −1.5), which are consistent with an origin involving crustal melting. Similar interpretations were reported for other strongly peraluminous A-type granites in the Sierras Pampeanas (e.g., the Achala batholith and Capilla del Monte pluton, Dahlquist et al., 2014, 2016).

Magmatic zircon grains in granites may display considerable ranges in $\varepsilon_{Hf,t}$ (particularly in peraluminous granites), with variations spanning up to 10ε units (e.g., Chen et al., 2015; Dahlquist et al., 2013; Farina et al., 2014; Kemp et al., 2007), i.e., about one order of magnitude greater than the common uncertainty on $\varepsilon_{Hf,t}$ determination. Such $\varepsilon_{Hf,t}$ variability has been the subject of intense and controversial discussion in these last years (e.g., Chen et al., 2015; Farina et al., 2014; Kemp et al., 2007; Villaros et al., 2012). In particular, the U–Pb and Hf isotopic analyses of zircon grains in granites with metasedimentary source revealed that the highly variable $\varepsilon_{Hf,t}$ values may be source-inherited, reflecting mixing of a range of crustal materials of different ages and original isotopic signatures (Villaros et al., 2012). Farina et al. (2014) gave some new insight into the process responsible for Hf isotope variability in zircons from S-type granites. They suggested that the dissolution rate, size and distribution of zircon crystals and the crystallization rate of magmas are the important parameters controlling the Hf isotope composition of newly grown magmatic zircons. In other words, the Hf isotope variability of syn-magmatic zircons is primarily dictated by the ε_{Hf} variability and spatial distribution of relict or inherited zircons in the host magmas.

Our $\varepsilon_{Hf,t}$ range of values from the granites of the Sierra de Vinquis can be interpreted in a similar way. Thus, the dominant $\varepsilon_{Hf,t}$ values ranging from −4.9 to −6.8 can be assumed as the main contribution to the melt of dominant inherited zircons (Cambrian and Ordovician) from the protolith (Fig. 9). Two 'anomalous' $\varepsilon_{Hf,t}$ values for magmatic zircons (−1.5 and −9.5) may be the result of occasional inherited zircons with high and low $^{176}Hf/^{177}Hf$ ratios, respectively.

The $\varepsilon_{Nd,t}$ values of the studied granitic rocks (ranging from −6.1 to −7.8) are fully consistent with the dominant $\varepsilon_{Hf,t}$ range values, showing an appropriate coupling between both isotope systems. This observation suggests that Hf from non-zircon minerals was scarce or absent (as suggested by Chen et al., 2015; Tang et al., 2014). The breakdown of Hf-bearing major minerals (especially garnet) in anatectic reactions causes the dissolution of Hf into such melts, resulting in elevated $^{176}Hf/^{177}Hf$ ratios (Chen et al., 2015). Hf contributions from non-zircon minerals such as garnet lead to Nd–Hf isotopic decoupling (Tang et al., 2014).

When the $\varepsilon_{Hf,t}$ of Cambrian and Ordovician inherited zircon from the Vinquis granite is calculated at t = 355 Ma, similar values are obtained to the dominant $\varepsilon_{Hf,t}$ values reported for zircons that crystallized at that time. The most direct interpretation of this similarity is that the Vinquis batholith magma resulted mainly from reworking of supracrustal material.

The average of three depleted mantle Nd model ages is 1.66 Ga (n = 3), essentially coincident with the Hf model age (1.69 Ga; n = 9). These data are suggestive of a dominant Mesoproterozoic continental lithosphere source. The whole-rock composition and these isotopic data preclude a direct asthenospheric mantle contribution in the generation of the parental magma.

7.3. Petrogenesis of the granitic magmas

Granites of the Vinquis batholith mostly have restricted monzogranite composition, with distinctive high ASI values. The occurrence of magmatic muscovite and occasional sillimanite and garnet is consistent with the high ASI values. Based on these characteristics the granites of the Vinquis batholith can be classified as strongly peraluminous according to the definition of Zen (1988).

The zircon saturation thermometry of Watson and Harrison (1983) provides a simple and robust means of estimating magma temperatures for both metaluminous and peraluminous rocks, either inheritance-rich or inheritance-poor (Miller et al., 2003). The calculated results for M values between 1.17 and 1.32 (the calibration range for the geothermometer) range from 685 °C to 803 °C (Table 7), which are

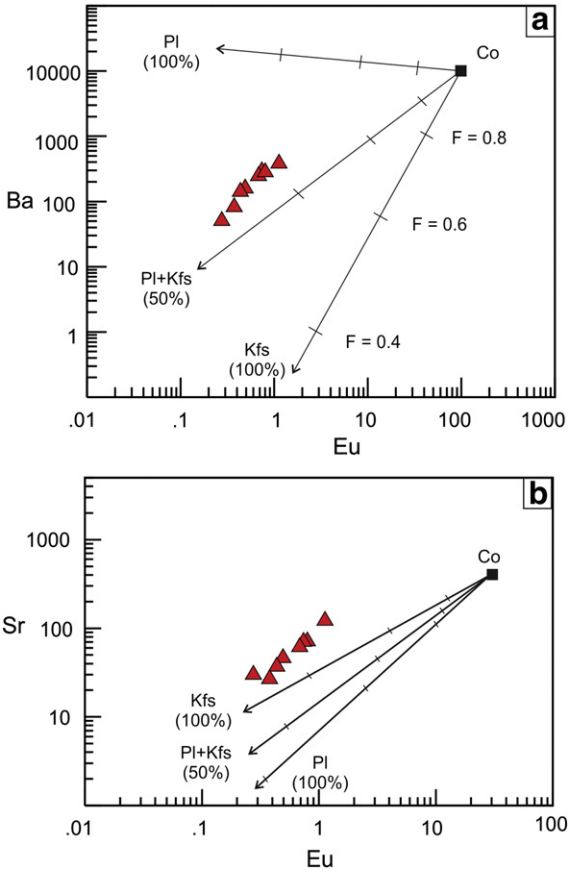

Fig. 11. (a) Ba vs. Eu and (b) Sr vs. Eu. Linear trends for eight granitic samples of the Vinquis batholith indicate that K-feldspar (Kfs) and plagioclase (Pl) crystallize in an approximately 50:50 ratio. The partition coefficient data for minerals in equilibrium with granitic liquids are from Dahlquist et al. (2014). The crystallization percentage for Kfs and Pl is indicated in the figure. Co = Initial concentration, F = weight fraction of remaining melt.
(Modified from Dahlquist et al., 2014.)

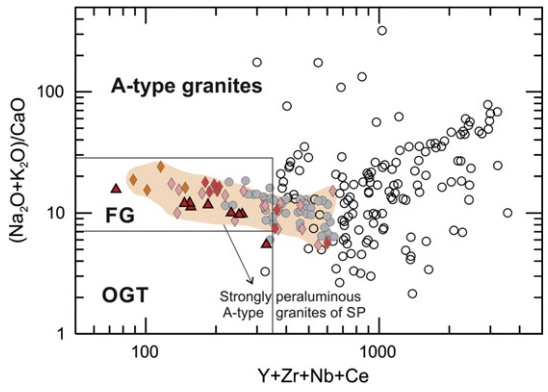

Fig. 12. ($K_2O + Na_2O$)/CaO vs. Zr + Nb + Ce + Y discrimination diagram for A-type granites, fractionated felsic granites (*FG*) and unfractionated M-, I- and S-type granites (*OGT*) from Whalen et al. (1987), showing the compositions of the studied granites of the Vinquis batholith and metaluminous and strongly peraluminous A-type granite of Sierras Pampeanas reported in the Fig. 13. Data sources reported in Fig. 3. New data is from Eby (1992) (empty circles).

quite typical for granites. A crude correlation shows that the temperature decreases as the SiO_2 content increases (Table 7), as might be expected.

Chondrite-normalized REE plots and primitive-mantle normalized spider diagrams show several distinctive features. (1) REE patterns tend to be smooth and slightly LREE-enriched and have significant negative Eu anomalies, indicating that feldspar fractionation or residual feldspar in the source region played a relevant role in the petrogenesis of the magmas (Fig. 6a). (2) Significant negative Ba and Sr anomalies and positive Rb and Cs anomalies in the spider diagrams similarly demonstrate the important role of feldspar and biotite (Fig. 6b). (3) Significant negative Ti and positive P anomalies indicate that Ti oxides, apatite, and monazite also played a role. (4) LIL elements are significantly enriched with respect to primitive mantle, suggesting an important continental contribution.

Logarithmic plots of Eu versus Ba and Sr concentrations show linear trends for the granitic rocks of the Vinquis batholith (Fig. 11a, b). Both Ba and Sr decrease with decreasing Eu, showing the role of feldspar fractionation in the evolution of these magmas. Simple vectors calculated for Ba, Sr and Eu produce linear trends for a number of the samples, indicating (in agreement with the Rb and Cs increase), varying degrees of K-feldspar and plagioclase segregation through the crystallization process, as has been suggested for other A-type of Sierras Pampeanas (Dahlquist et al., 2010a; Dahlquist et al., 2016). Feldspar fractionation plays an important role in the evolution of A-type granite worldwide (e.g., Dall'Agnol et al., 2005; Deng et al., 2016; Eby, 1990; King et al., 2001; Vallinayagam and Kochhar, 2011; Whalen et al., 1987).

A strong positive correlation is observed between TiO_2 and MgO + FeO^t ($R^2 = 0.98$, excluding a fine-grained monzogranitic enclave reported in Section 4.2.1, data in Table 7). Considering that biotite is the sole ferromagnesian mineral present in these granites, this suggests removal of biotite and maybe ±Ti oxides. The concomitant decreases in LREE (La, Ce), Zr (Hf), and Th relative to FeO^t + MgO ($R^2 = 0.98$, again excluding the enclaves) suggest the segregation of accessory minerals such as zircon and monazite as well as biotite (Fig. 7a,b). Fractionation of similar accessory minerals has been reported for A-type granites (e.g., Dahlquist et al., 2010a; Dahlquist et al., 2016; Eby, 1990; King et al., 2001).

In general, the A-type granites are characterized by relatively high HFSE (Whalen et al., 1987) (e.g., Zr + Nb + Ce + Y > 350 ppm), although there are exceptions (Bonin, 2007). The granites of the Vinquis batholith have lower HFSE content than the metaluminous A-type of the Sierras Pampeanas (Dahlquist et al., 2010a) and other classic A-type granites worldwide (e.g., Eby, 1992; Whalen et al., 1987 and references therein) (Fig. 12).

A high concentration of P_2O_5 is a common feature of the Achala and Vinquis batholiths in contrast to the metaluminous to weakly peraluminous Early Carboniferous A-type granites of Sierras Pampeanas (Dahlquist et al., 2010a) (Fig. 13). For the Achala batholith Dahlquist et al. (2014) suggested that the high P_2O_5 content is consistent with a mainly metasedimentary continental source, P (together with volatile elements such as F) is a common element in some sedimentary rocks (e.g., Gromet et al., 1984; Nelson, 1992; Taylor and McLennan, 1985). The initially high phosphorus contents of metapelitic protoliths is especially reflected in the peraluminous granitic melts that they produce, because the solubility of the phosphorus increases in peraluminous compositions (Villaseca et al., 2008). Additionally, the conspicuous presence of tourmaline in some granitic facies of the Vinquis batholith would suggests the presence of boron in the source and is consistent with a pelitic metasedimentary one.

However, an alternative mechanism can be invoked to explain the high P_2O_5 content (Fig. 13) and several geochemical peculiarities of the Vinquis batholith (e.g., the low abundance of HFSE). The behavior of Zr, REE, Y, Th, and U during felsic crustal processes is mostly controlled by four accessory minerals (monazite, xenotime, apatite and

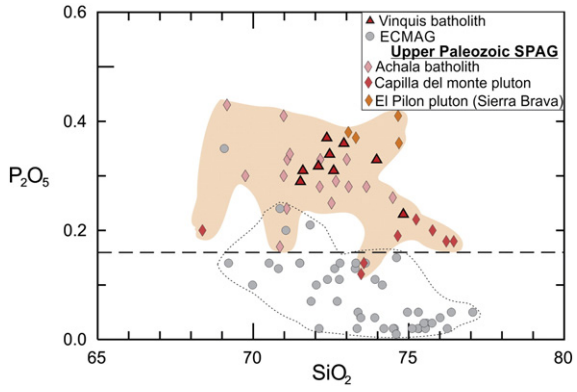

Fig. 13. P_2O_5 vs. SiO_2 wt.% granite discrimination diagram showing granites of the Vinquis batholith compared to the metaluminous to weakly peraluminous Early Carboniferous A-type granites (ECMAG) and Upper Paleozoic strongly peraluminous A-type granites (SPAG) of Sierras Pampeanas. Boundary line is approximated. Data sources are reported in Fig. 3.

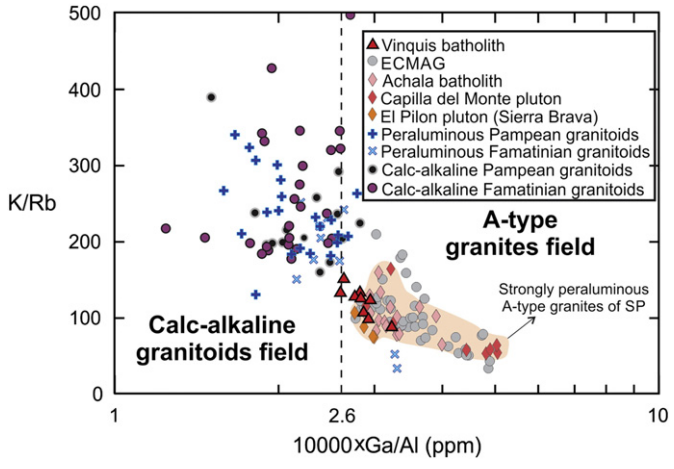

Fig. 14. K/Rb vs. 10,000 × Ga/Al granite discrimination diagram (modified from Rapela et al., 2008b) showing the compositions of the studied granites from the Vinquis batholith, calc-alkaline granites, and metaluminous and strongly peraluminous A-type granites (see references for granitic rocks in inset). The 10,000 × Ga/Al discrimination limit for A-type granites is from Whalen et al. (1987). Chemical data for A-type granites of Sierras Pampeanas are reported in Fig. 3. Chemical data for the Pampean and Famatinian granitoids are from Dahlquist et al. (2005), Grosse et al. (2011), Iannizzotto et al. (2013), Pankhurst et al. (1998, 2000), and Rapela et al. (1998, 2002).

zircon) that usually account for at least 80–90% of the total budget of these elements in crustal rocks (e.g., Bea, 1996). Metaluminous and strongly peraluminous A-type granites in the Sierras Pampeanas show a contrasting behavior of HFSE and P_2O_5 which can be linked to their ASI. The solubility of accessory phases is reasonably well known due to a considerable body of experimental data (e.g., Watson, 1996; Wolf and London, 1994; Wolf and London, 1995 and references therein), and show that ASI constrains the solubility of different accessory minerals during partial melting. In particular, apatite has an elevated solubility in peraluminous melts, while zircon, monazite, and xenotime have significantly reduced solubility. Therefore, the ASI in metaluminous and strongly peraluminous A-type granites constrains the concentration of some trace elements in the parental melt (Fig. 12). Remarkably, those trace elements highly fractionated by feldspar or biotites (such as Rb, Sr, Ba, Cs, Ga) have similar concentrations in metaluminous and strongly peraluminous A-type granites.

In summary, the parallel development of negative Ba and Sr and positive Rb and Cs anomalies in the spider diagram and Eu anomalies in the REE diagram (Fig. 6a,b), as well as the logarithmic plots of Eu versus Ba and Sr (Fig. 11), is consistent with dominant feldspar fractionation. The TiO_2, LREE, Th, Zr and Hf vs MgO + FeO^t diagrams suggest segregation of biotite and associated accessory minerals such as Ti oxides, zircon and monazite. The lower LREE, Th, Zr, Hf and higher P_2O_5 relative to A-type metaluminous granites could result from the degree of solubility of accessory minerals during the partial melting process, constrained by the ASI of the melt. This compositional behavior linked to ASI and has been reported for others felsic granites (Breiter, 2012; Champion and Bultitude, 2013; Chappell, 1999; Sawka et al., 1990).

High Ga/Al values are a distinctive characteristic of A-type granite, and plots against major and trace element contents can readily distinguish between I-type (calc-alkaline), S-type and A-type granite (Whalen et al., 1987). Using the K/Rb vs. Ga/Al diagram (Fig. 14), strongly peraluminous A-type granites of the Vinquis batholith and the Carboniferous and Devonian granites of the Sierras Pampeanas (both metaluminous and peraluminous) are distinct from Cambrian (Pampean orogeny) and Ordovician (Famatinian orogeny) metaluminous calc-alkaline and peraluminous granites emplaced in the pre-Andean margin of Gondwana.

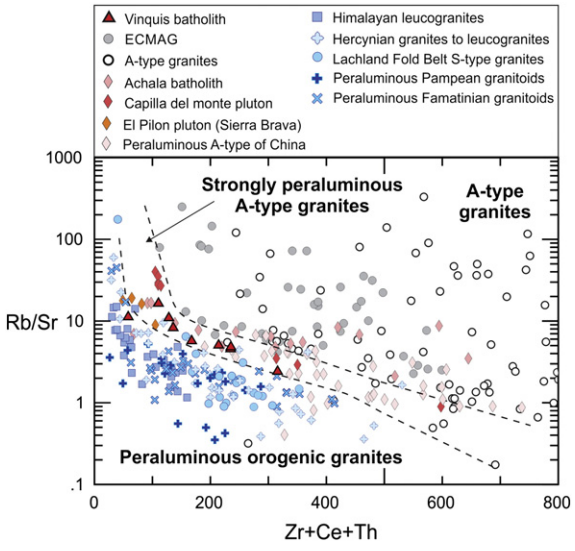

Fig. 15. Rb/Sr vs. Zr + Ce + Th granite discrimination diagram showing the compositions of the studied granites from the Vinquis batholith, peraluminous orogenic granites and metaluminous and strongly peraluminous A-type granites (see references for granitic rocks in the inset). Data sources reported in previous figures. New data is from Chappell and White (1992), Downes et al. (1997), Guo and Wilson (2012), Healy et al. (2004), Merino Martínez et al. (2014), Sun et al. (2011), Williamson et al. (1996), Shellnutt and Zhou, (2007), Sun et al., (2011), Xia et al., (2012) and Feng et al., (2014).

Experimental studies by Patiño Douce (1997) indicate that the higher proportion of Ca-rich plagioclase formed by incongruent melting at low-pressure (4 kbar) explains the low CaO relative to Al_2O_3 of metaluminous A-type granites (as well as their Eu depletion), and because plagioclase excludes Ga relative to Al_2O_3 (Malvin and Drake, 1987), it also gives rise to their distinctively high Ga/Al values. The low Ca concentration in the magma during the crystallization process is evident from the very sodic plagioclase composition (Ab_{84-96}, Table 1). Alternatively, Whalen et al. (1987) indicated that Ga is enriched relative to Al because the latter is preferentially trapped in residual plagioclase, while during melting of an F-enriched source Ga is stabilized in the melt as GaF_6^{-3}. The high F content is evident from mineral chemistry of biotite (see Section 4.2.2).

In a Rb/Sr vs. Th + Zr + Ce diagram (Fig. 15), the granites of the Vinquis batholith and the Late Devonian and Early Carboniferous strongly peraluminous A-type granites of the Sierras Pampeanas are distinguished from: i) world examples of orogenic strongly peraluminous granites (S-type or two-mica granites, e.g., Himalayan and the European Hercynian belt granites), ii) S-type granites of the Lachlan Fold Belt, iii) local examples of orogenic strongly peraluminous granites (i.e. Famatinian and Pampean orogenic granites), and iv) metaluminous to weakly peraluminous and peralkaline A-type granites. Only a few samples of strongly fractionated S-type granites (Chappell and White, 1992) plot within of the strongly peraluminous A-type granite field.

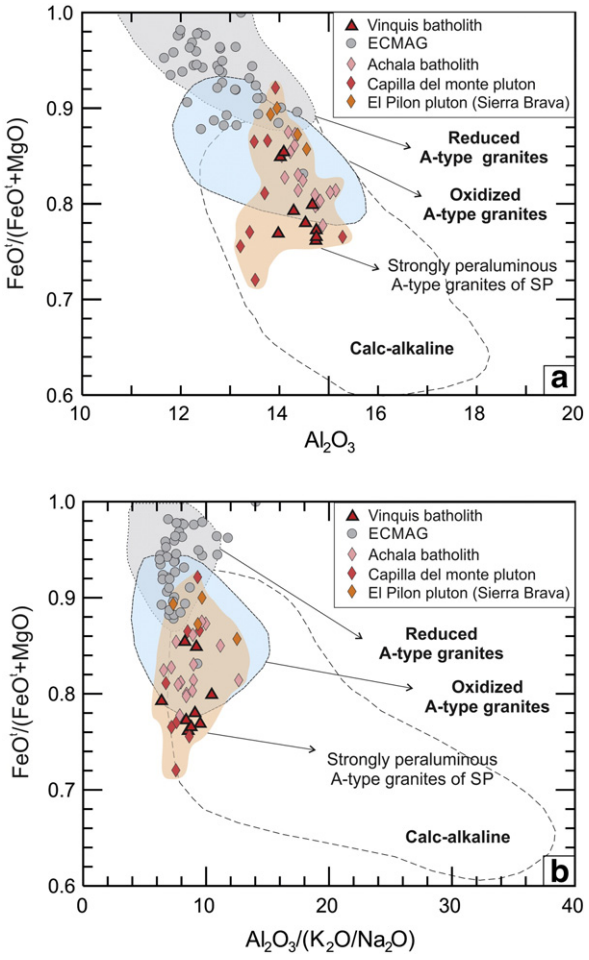

Fig. 16. Whole-rock $FeO^t/(FeO^t + MgO)$ vs. Al_2O_3 (a), and $FeO^t/(FeO^t + MgO)$ vs. $Al_2O_3/(K_2O/Na_2O)$ (b). Diagrams show the composition of representative oxidized and reduced A-type granites compared with calc-alkaline granites. Data sources are Dall'Agnol and Oliveira (2007) and data sources reported in Fig. 12.

7.4. Reduced and oxidized A-type granites

Experimental results indicate that the nature of A-type granites (besides other parameters such as pressure, metasomatized source, etc.) is strongly dependent on fO_2 conditions and the H_2O content of magma sources (Patiño Douce, 1999; Anderson and Morrison, 2005; Dall'Agnol and Oliveira, 2007; and references therein). As already noted, some authors have distinguished oxidized and reduced A-type granites. Anderson and Morrison (2005) have reported that whole-rock $FeO^t/(FeO^t + MgO)$ values of magnetite-series granites of Laurentia typically range between 0.80 and 0.88, whereas those of ilmenite-series granites are generally higher (>0.88). Similar differences are shown by Dall'Agnol and Oliveira (2007) for oxidized and reduced A-type granites. Early Carboniferous metaluminous to weakly peraluminous A-type granites of the Sierras Pampeanas (Dahlquist et al., 2010a) have a strong ferroan signature, with high whole-rock $(FeO^t/(FeO^t + MgO)$ values (0.83–0.98) compatible with the reduced A-type granites reported by Dall'Agnol and Oliveira (2007). The granites of the Vinquis batholith have $FeO^t/(FeO^t + MgO)$ ranging from 0.76 to 0.85, which is consistent with values reported by Dall'Agnol and Oliveira (2007) for oxidized A-type granites. Correspondingly, the strongly peraluminous A-type Vinquis and Capilla del Monte granites plot within the oxidized A-type granite field in Fig. 16a and b, whereas the Early Carboniferous metaluminous to weakly peraluminous A-type granites plot in the field of reduced granites. These relationships are consistent with those deduced from the $Fe^{2+}/(Fe^{2+} + Mg)$ values of biotite (Section 7.1).

The erratic and scarce presence of ilmenite and rutile would suggest early crystallization and segregation of magnetite relative to ilmenite, leading to a relative enrichment of Ti in the magma. Dall'Agnol and Oliveira (2007) reported magnetite-bearing granites with whole-rock and mineral chemistry that indicate crystallization in relatively reduced conditions. It seems that the presence of magnetite or ilmenite is not always a direct indicator of fO_2 in the magma although the reason for this ambiguous behavior is not clearly understood (see discussion in Dall'Agnol and Oliveira, 2007).

Oxidized A-type magmas are considered to be derived from melts with appreciable H_2O contents (≥4 wt.% H_2O) whereas reduced A-type granites may be derived from sources with low H_2O contents, perhaps as little as 2–3 wt.% H_2O (Dall'Agnol and Oliveira, 2007; Patiño Douce, 1997 and references therein). Various authors (e.g., Anderson and Morrison, 2005; Dall'Agnol and Oliveira, 2007) have shown that reduced A-type granites have the typical A-type geochemical signature whereas oxidized granites, although retaining A-type characteristics, have less pronounced A-type geochemical signature.

As noted in Section 7.3, experimental results by Patiño Douce (1997, 1999) indicate that the higher proportion of Ca-rich plagioclase and orthopyroxene formed by incongruent melting in low pressure conditions (4 kbar) and with low H_2O contents explains the typical geochemical signature of A-type granites (low CaO relative to Al_2O_3, high FeO/MgO ratios, etc.). Dall'Agnol and Oliveira (2007) conclude that high H_2O contents (≥4 wt.% H_2O) during melting favor the presence of residual clinopyroxene, and this can explain the less typical A-type geochemical signature of oxidized A-type granites.

A metasediment-rich source was postulated for two-mica A-type granites in the USA by Anderson and Morrison (1992). The metasedimentary source postulated for the Vinquis granites (Section 7.2) could account for an appreciable H_2O content in the source since this would be higher in metasedimentary material than in meta-igneous one.

7.5. Paleozoic metaluminous to weakly peraluminous and strongly peraluminous A-type granites of Sierras Pampeanas

Our previous studies (Dahlquist et al., 2010a; Dahlquist et al., 2016) indicate that during the Early Carboniferous, metaluminous and peraluminous A-type granites were emplaced in the intracontinental region of the pre-Andean margin of SW Gondwana (now the Eastern Sierras Pampeanas). Previously, Late Devonian peraluminous A-type granites (Dahlquist et al., 2014) were emplaced in the same region (Fig. 1).

The latest Devonian or earliest Carboniferous Vinquis granites have similarities with strongly peraluminous A-type granites of Sierras Pampeanas such as the Late Devonian Achala batholith (Dahlquist et al., 2014) and the Early Carboniferous Capilla del Monte pluton (Dahlquist et al., 2016) (see Figs. 3 to 6 and 12 to 16). In addition, the Vinquis granites show some minor geochemical differences from the Early Carboniferous metaluminous to weakly peraluminous A-type granites of the Sierras Pampeanas.

On the basis of the previous discussion we can conclude that metaluminous to weakly peraluminous and strongly peraluminous A-type granites were derived from two different sources, metaigneous and metasedimentary one, and that they crystallized synchronously in dominantly reduced and oxidized conditions, respectively. Both varieties were emplaced in a dominant extensional regimen as it was suggested by Dahlquist et al. (2016).

8. Conclusions

1. The Vinquis batholith was emplaced in latest Devonian or earliest Carboniferous time; U–Pb zircon dating yielded a crystallization age of 355 ± 7 (355 Ma correspond to earliest Tournaisian).
2. Considering previous works and the data reported here, emplacement of the Vinquis batholith was probably synchronous with Early Carboniferous metaluminous A-type granites in the pre-Andean intracontinental region of SW Gondwana.
3. Based on the geochemical data reported here, the Vinquis batholith can be classified as a F-rich strongly peraluminous A-type granite, a singular and distinctive subtype of A-type granites.
4. The whole-rock and mineral chemistry of the granites of the Vinquis batholith indicate that the magma crystallized under dominantly oxidizing conditions whereas the Early Carboniferous metaluminous to weakly peraluminous A-type granites of the Sierras Pampeanas crystallized under dominantly reduced conditions.
5. The contrasting behavior of HFSE and P_2O_5 observed for metaluminous and strongly peraluminous A-type granites can be linked to the ASI of the melt, which constrains the solubility of accessory minerals such as apatite, zircon, monazite, and xenotime during partial melting.
6. Both Hf and Nd-isotopes data indicate that the source of the parental magma was old continental crust with dominant metasedimentary material enriched in P and volatiles such as F, B.
7. Following previous work (see Section 7.2) the dominant $\varepsilon_{Hf,t}$ values can be explained by $^{176}Hf/^{177}Hf$ transfer from Cambrian and Ordovician inherited zircon to magmatic zircon crystallized in the granites of the Vinquis batholith. Anomalous values would be explained by $^{176}Hf/^{177}Hf$ transfer from scattered inherited zircons of unknown age. Systematic studies of the Hf content in zircons are required to elucidate this issue.
8. The geochemical evidence indicates that differentiation of the granitic rocks occurred by mineral fractionation from a F-rich peraluminous parental magma, dominantly of plagioclase, K-feldspar, biotite, and accessory minerals such as zircon, monazite, xenotime, and oxides.
9. The Rb/Sr vs. Th + Zr + Ce plot is an appropriate discriminator diagram that permits distinction between strongly peraluminous A-type granites, metaluminous and peralkaline A-type granites and strongly peraluminous orogenic granites.

Supplementary data to this article can be found online at http://dx.doi.org/10.1016/j.lithos.2016.10.035.

Acknowledgments

Financial support was provided by Grant CONICET-FAPESP 2013–2014, FONCyT PICT-2013 0226, and SECyT-UNC 2014-2015 (Res. Rec. 1565). We greatly appreciate the detailed and constructive review and editorial work carried out on the manuscript by R. Martin, two anonymous reviewers, and the Associate Editor Ed Sawyer, which have improved greatly the manuscript. We are also grateful to V. Loios, W. Sproesser, S. Souza, N. Coelho, F. Colombo and S. Verdecchia for the technical support. Finally, we greatly appreciate the English revision of the manuscript by R.J. Pankhurst.

References

Abdel Rahman, A.M., 1994. Nature of biotites from alkaline, calc-alkaline, and peraluminous magmas. Journal of Petrology 35, 525–541.

Alasino, P.H., Dahlquist, J.A., Galindo, C., Casquet, C., Saavedra, J., 2010. Andalusite and Na- and Li-rich cordierite in the La Costa pluton, Sierras Pampeanas, Argentina: textural and chemical evidence for a magmatic origin. International Journal of Earth Sciences 99, 1051–1065.

Alasino, P.H., Dahlquist, J.A., Pankhurst, R.J., Galindo, C., Casquet, C., Rapela, C.W., Larrovere, M., Fanning, C.M., 2012. Early Carboniferous sub- to mid-alkaline magmatism in the Eastern Sierras Pampeanas, northwestern Argentina: a record of crustal growth by the incorporation of mantle derived material in an extensional setting. Gondwana Research 22, 992–1008.

Alasino, P.H., Casquet, C., Pankhurst, R.J., Rapela, C.W., Dahlquist, J.A., Galindo, C., Larrovere, M., Recio, C., Paterson, S., Colombo, F., Baldo, E.G., 2016. Mafic rocks of the Ordovician Famatinian magmatic arc (NW Argentina): new insights into the mantle contribution. Geological Society of America Bulletin 128 (7/8), 1105–1120.

Anderson, J.L., Bender, E.E., 1989. Nature and origin of Proterozoic A-type granitic magmatism in the southwestern United States of America. Lithos 23, 19–52.

Anderson, J.L., Morrison, J., 1992. The role of anorogenic granites in the Proterozoic crustal development of North America. In: Condie, K.C. (Ed.), Proterozoic Crustal Evolution. Elsevier, Amsterdam, pp. 263–299.

Anderson, J.L., Morrison, J., 1998. Oxygen isotope systematics of 1.3 to 1.6 Ga granites of Laurentia. Abstracts with Programs - Geological Society of America 30, A89.

Anderson, J.L., Morrison, J., 2005. Ilmenite, magnetite, and peraluminous Mesoproterozoic anorogenic granites of Laurentia and Baltica. Lithos 80, 45–60.

Anderson, J.L., Smith, D.R., 1995. The effects of temperature and fO_2 on the Al-inhornblende barometer. American Mineralogist 80, 549–559.

Anderson, J.L., Thomas, W.M., 1985. Proterozoic anorogenic two mica granites: silver plume and St. Vrains batholiths of Colorado. Geology 13, 177–180.

Ávila, J., Lazarte, J.E., Gianfrancisco, M., Fogliata, A.S., 1999. Metalogénesis de wolframio y estaño de Catamarca. En: Recursos minerales de la República Argentina, Instituto de Geología y Recursos Minerales SEGEMAR. Anales 35, 563–573.

Barker, F., Wones, D.R., Sharp, W.N., Desborough, G.A., 1975. The Pikes Peak batholith, Colorado Front Range, and a model for the origin of the gabbro–anorthosite–syenite–potassic granite. Precambrian Research 2, 97–160.

Barnes, C.G., Yoshinobu, A.S., Prestvik, T., Nordgulen, Ø., Karlsson, H.R., Sundvoll, B., 2002. Mafic magma intraplating: anatexis and hybridization in arc crust, Bindal batholith, Norway. Journal of Petrology 43, 2171–2190.

Bea, F., 1996. Residence of REE, Y, Th and U in granites and crustal protoliths: implications for the chemistry of crustal melts. Journal of Petrology 37, 521–552.

Bonin, B., 2007. A-type granites and related rocks: evolution of a concept, problems and prospects. Lithos 97, 1–29.

Boynton, W.V., 1984. Geochemistry of the rare earth elements: meteorites studies. In: Henderson, P. (Ed.), Rare Earth Element Geochemistry. Elsevier, pp. 63–114.

Breiter, K., 2012. Nearly contemporaneous evolution of the A- and S-type fractionated granites in the Krušné hory/Erzgebirge Mts., Central Europe. Lithos 151, 105–121.

Casquet, C., Rapela, C., Pankhurst, R., Baldo, E., Galindo, C., Verdeccia, S., Dahlquist, J., Murra, J., Fanning, M., 2012. A post Pampean Middle to Late Cambrian siliciclastic platform on the proto-Andean margin of Gondwana and its paleogeographical implications. Simposio de Geología de la Cordillera de Los Andes y su antepaís. Congreso Geológico de España, No. 8. Geo-Temas. Vol. 13, pp. 1852–1855 (España).

Cawood, P.A., 2005. Terra Australis orogen: Rodinia breakup and development of the Pacific and Iapetus margins of Gondwana during the Neoproterozoic and Paleozoic. Earth-Science Reviews 69, 249–279.

Champion, D.C., Bultitude, R.J., 2013. The geochemical and Sr–Nd isotopic characteristics of Paleozoic fractionated S-types granites of north Queensland: implications for S-type granite petrogenesis. Lithos 162-163, 37–56.

Chappell, B.W., 1999. Aluminium saturation in I- and S-type granites and the characterization of fractionated haplogranites. Lithos 46, 535–551.

Chappell, B.W., White, A.J.R., 1992. I- and S-type granites in the Lachlan Fold Belt. Transactions of the Royal Society of Edinburgh: Earth Sciences 83, 1–26.

Chen, Y.X., Gao, P., Zheng, Y.F., 2015. The anatectic effect on the zircon Hf isotope composition of migmatites and associated granites. Lithos 238, 174–184.

Clarke, D.B., Dorais, M., Barbarin, B., Barker, D., Cesare, B., Clarke, G., el Baghdadi, M., Erdmann, S., Förster, H.-J., Gaeta, M., Gottesmann, B., Jamieson, R.A., Kontak, D.J., Koller, F., Gomes, C.L., London, D., Morgan, V.I.G.B., Neves, L.J.P.F., Pattison, D.R.M., Pereira, A.J.S.C., Pichavant, M., Rapela, C., Renno, A.D., Richards, S., Roberts, M., Rottura, A., Saavedra, J., Sial, A.N., Toselli, A.J., Ugidos, J.M., Uher, P., Villaseca, C., Visona, D., Whitney, D.L., Williamson, B., Woodard, H.H., 2005. Occurrence and origin of andalusite in peraluminous felsic igneous rocks. Journal of Petrology 46, 441–472.

Dahlquist, J.A., Alasino, P.H., 2012. Primera edad U–Pb en circón usando LA-ICP-MS de un dique traquiandesítico emplazado en el granito tipo-A Los Árboles, Sierras Pampeanas Orientales. Revista de la Asociación Geológica Argentina 69 (2), 296–299.

Dahlquist, J.A., Rapela, C.W., Baldo, E.G., 2005. Petrogenesis of cordierite-bearing S-type granitoids in Sierra de Chepes, Famatinian orogen, Argentina. Journal of South American Earth Sciences 20, 231–251.

Dahlquist, J.A., Alasino, P.H., Galindo, C., Pankhurst, R.J., Rapela, C.W., Saavedra, J., Casquet, C., Baldo, E.G., González Casado, J.M., 2006. Evolución magmática del granito Peñón Rosado, cerro Asperecito, flanco occidental de la sierra de Famatina. Revista de la Asociación Geológica Argentina 61, 93–111.

Dahlquist, J.A., Galindo, C., Pankhurst, R.J., Rapela, C.W., Alasino, P.H., Saavedra, J., Fanning, C.M., 2007. Magmatic evolution of the Peñón Rosado granite: petrogenesis of garnet-bearing granitoids. Lithos 95, 177–207.

Dahlquist, J.A., Pankhurst, R.J., Rapela, C.W., Galindo, C., Alasino, P., Fanning, C.M., Saavedra, J., Baldo, E., 2008. New SHRIMP U–Pb data from the Famatina complex: constraining Early-Mid Ordovician Famatinian magmatism in the Sierras Pampeanas, Argentina. Geologica Acta 6, 319–333.

Dahlquist, J.A., Colombo, F., Murra, J.A., Locati, F., Alasino, P.H., Baldo, E., Verdecchia, S., 2010b. El stock álcali-feldespático El Pilón (Sierra Brava, La Rioja): un ejemplo de magmatismo granítico turmalinífero. Revista de la Asociación Geológica Argentina 67 (3), 369–382.

Dahlquist, J.A., Pankhurst, R.J., Gaschnig, R.M., Rapela, C.W., Casquet, C., Alasino, P.H., Galindo, C., Baldo, E., 2013. Hf and Nd isotopes in Early Ordovician to Early Carboniferous granites as monitors of crustal growth in the Proto-Andean margin of Gondwana. Gondwana Research 23, 1617–1630.

Dahlquist, J.A., Alasino, P.H., Bello, C., 2014. Devonian F-rich peraluminous A-type magmatism in the protoAndean foreland (Sierras Pampeanas, Argentina): geochemical constraints and petrogenesis from the western-central region of the Achala batholiths. Mineralogy and Petrology 108, 391–417.

Dahlquist, J.A., Alasino, P.H., Morales Cámera, M.M., 2015. Petrografía, química mineral y geoquímica comparada de los plutones Potrerillos y Cerro La Gloria: magmatismo de arco y retroarco en el carbonífero inferior. Revista de la Asociación Geológica Argentina 72 (2), 167–181.

Dahlquist, J.A., Pankhurst, R.J., Rapela, C.W., Basei, M.A., Alasino, P.H., Saavedra, J., Baldo, E.G., Murra, J.A., da Costa Campos Neto, M., 2016. The Capilla del Monte pluton, Sierras de Córdoba, Argentina: the easternmost Early Carboniferous magmatism in the pre-Andean SW Gondwana margin. International Journal of Earth Sciences 105, 1287–1305.

Dahlquist, J.A., Alasino, P.H., Eby, G.N., Galindo, C., Casquet, C., 2010a. Fault controlled Carboniferous A-type magmatism in the proto-Andean foreland (Sierras Pampeanas, Argentina): geochemical constraints and petrogenesis. Lithos 115, 65–81.

Dall'Agnol, R., Frost, C.D., Ramo, T., 2012. IGCP Project 510 "A-type granites and related rocks through time": project vita, results and contribution to granite research. Lithos 151, 1–16.

Dall'Agnol, R., Oliveira, D.C., 2007. Oxidized, magnetite-series, rapakivi-type granites of Carajás, Brazil: implications for classification and petrogenesis of A-type granites. Lithos 93, 215–233.

Dall'Agnol, R., Pichavant, M., Champenois, M., 1997a. Iron–titanium oxide mineral of the Jamon granite, Eastern Amazonian region, Brazil: implications for the oxygen fugacity in Proterozoic A-type granites. Anais da Academia Brasileira de Ciências 69, 325–347.

Dall'Agnol, R., Rämö, O.T., Magalhães, M.S., Macambira, M.J.B., 1999a. Petrology of the anorogenic, oxidised Jamon and Musa granites, Amazonian craton: implications for the genesis of Proterozoic A-type granites. Lithos 46, 431–462.

Dall'Agnol, R., Scaillet, B., Pichavant, M., 1999b. An experimental study of a Lower Proterozoic A-type granite from the Eastern Amazonian craton, Brazil. Journal of Petrology 40, 1673–1698.

Dall'Agnol, R., Scaillet, B., Pichavant, M., 1999c. An experimental study of a Lower Proterozoic A-type granite from the Eastern Amazonian craton, Brazil. Journal of Petrology 40, 1673–1698.

Dall'Agnol, R., Teixeira, N.P., Rämö, O.T., Moura, C.A.V., Macambira, M.J.B., Oliveira, D.C., 2005. Petrogenesis of the Paleoproterozoic, rapakivi, A-type granites of the Archean Carajás Metallogenic Province, Brazil. Lithos 80, 101–129.

de La Roche, H., 1992. Un homologue cationique du triangle Q–A–P (quartz–feldspath alcalin–plagioclase), figure majeure de la pétrologie des roches plutoniques. Comptes Rendus de l'Académie des Sciences, París, Série II 315, 1687–1693.

Deer, W.A., Howie, R.A., Zussman, J., 1992. An Introduction to the Rock Forming Minerals. Second Longman Editions. Longman, London, p. 696.

Deng, X., Zhao, T., Peng, T., 2016. Age and geochemistry of the early Mesoproterozoic A-type granites in the southern margin of the North China craton: constraints on their petrogenesis and tectonic implications. Precambrian Research 283, 68–88.

De Paolo, D.J., Linn, A.M., Schubert, G., 1991. The continental crustal age distribution; methods of determining mantle separation ages from Sm–Nd isotopic data and application to the Southwestern United States. Journal of Geophysical Research 96, 2071–2088.

Dorais, M., Lira, R., Chen, Y., Tingey, D., 1997. Origin of biotite–apatite-rich enclaves, Achala batholith, Argentina. Contributions to Mineralogy and Petrology 130, 31–46.

Downes, H., Shaw, A., Williamson, B.J., Thirlwall, M.F., 1997. Sr, Nd and Pb isotopic evidence for the lower crustal origin of Hercynian granodiorites and monzogranites, Massif Central, France. Chemical Geology 136, 99–122.

Ducea, M.N., Otamendi, J.E., Bergantz, G., Stair, K.M., Valencia, V.A., Gehrels, G.E., 2010. Timing constraints on building an intermediate plutonic arc crustal section: U–Pb

zircon geochronology of the Sierra Valle Fértil–La Huerta, Famatinian arc, Argentina. Tectonics 29, 21–22.
Eby, G.N., 1990. The A-type granitoids: a review of their occurrence and chemical characteristics and speculations on their petrogenesis. Lithos 26, 115–134.
Eby, G.N., 1992. Chemical subdivision of the A-type granitoids: petrogenetic and tectonic implications. Geology 20, 641–644.
Farina, F., Stevens, G., Gerdes, A., Frei, D., 2014. Small-scale Hf isotopic variability in the peninsula pluton (South Africa): the processes that control inheritance of source 176Hf/177Hf diversity in S-type granites. Contributions to Mineralogy and Petrology 168, 1–18.
Feng, S.J., Zhao, K.D., Ling, H.F., Chen, P.R., Chen, W.F., Sun, T., Jiang, S.Y., Pu, W., 2014. Geochronology, elemental and Nd–Hf isotopic geochemistry of Devonian A-type granites in central Jiangxi, South China: constraints on petrogenesis and post-collisional extension of the Wuyi–Yunkai orogeny. Lithos 206-207, 1–18.
Frost, C.D., Frost, B.R., 2011. On ferroan (A-type) granites: their compositional variability and modes of origin. Journal of Petrology 52, 39–53.
Frost, B.R., Barnes, C.G., Collins, W.J., Arculus, R.J., Ellis, D.J., Frost, C.D., 2001. A geochemical classification for granitic rocks. Journal of Petrology 42, 2033–2048.
Gonzalez Bonorino, F., 1972. Descripción Geológica de la Hoja 13c, Fiambalá, Provincia de Catamarca. Subsecretaría de Minería de Buenos Aires.
Gromet, L.P., Dymek, R.F., Haskin, L.A., Korotev, R.L., 1984. The "North American shale composite": its compilation, major and trace element characteristics. Geochimica et Cosmochimica Acta 48, 2469–2482.
Grosse, P., Söllner, F., Báez, M.A., Toselli, A.J., Rossi, J.N., de la Rosa, J.D., 2009. Lower Carboniferous post-orogenic granites in central-eastern Sierra de Velasco, Sierras Pampeanas, Argentina: U-Pb monazite geochronology, geochemistry and Sr-Nd isotopes. International Journal of Earth Sciences 98, 1001–1025.
Grosse, P., Bellos, L.I., de los Hoyos, C.R., Larrovere, M.A., Rossi, J.N., Toselli, A.J., 2011. Across-arc variation of the Famatinian magmatic arc (NW Argentina) exemplified by I-, S- and transitional I/S-type Early Ordovician granitoids of the Sierra de Velasco. Journal of South American Earth Sciences 32, 110–126.
Guo, Z., Wilson, M., 2012. The Himalayan leucogranites: constraints on the nature of their crustal source region and geodynamic setting. Gondwana Research 22, 360–376.
Healy, B., Collins, W.J., Richards, S.W., 2004. A hybrid origin for Lachlan S-type granites: the Murrumbidgee batholith example. Lithos 78, 197–216.
Höckenreiner, M., Söllner, F., Miller, H., 2003. Dating the TIPA shear zone: an early Devonian terrane boundary between the Famatinian and Pampean systems (NW Argentina). Journal of South American Earth Sciences 16, 45–66.
Iannizzotto, N.F., Rapela, C.W., Baldo, E.G., Galindo, C., Fanning, C.M., Pankhurst, R.J., 2013. The Sierra Norte-Ambargasta batholith: Late Ediacaran-Early Cambrian magmatism associated with Pampean transpressional tectonics. Journal of South American Earth Sciences 42, 127–143.
Johansson, Å., Waight, T., Andersen, T., Simonsen, S.L., 2016. Geochemistry and petrogenesis of Mesoproterozoic A-type granitoids from the Danish island of Bornholm, southern Fennoscandia. Lithos 244, 94–108.
Jordan, T.E., Allmendinger, R.O., 1986. The Sierras Pampeanas of Argentina; a modern analogue to the Rocky Mountain Foreland deformation. American Journal of Earth Science 286, 737–768.
Kemp, A.I.S., Hawkesworth, C.J., Foster, G.L., Paterson, G.A., Woodhead, J.D., Hergt, J.M., Gray, C.M., Whitehouse, M.J., 2007. Magmatic and crustal differentiation history of granitic rocks from Hf–O isotopes in zircon. Science 315, 980–983.
King, P.L., White, A.J.R., Chappell, B.W., Allen, C.M., 1997. Characterization and origin of aluminous A-type granites from the Lachlan Fold Belt, southeastern Australia. Journal of Petrology 38, 371–391.
King, P.L., Chappell, B.W., Allen, C.M., White, A.J.R., 2001. Are A-type granites the high-temperature felsic granites? Evidence from fractionated granites of the Wangrah Suite. Australian Journal of Earth Sciences 48, 501–514.
Larrovere, M.A., Alasino, P.H., Baldo, E.G., 2016. La faja de cizalla dúctil doble-vergente del noroeste de la sierra de velasco: deformación de la corteza media durante la orogenia famatiniana. Revista de la Asociación Geológica Argentina 73 (1), 117–133.
Lazarte, J.E., 2013. Granitoides peraluminosos de mina San Antonio (tungsteno), Sierra de Vinquis norte, Sierras Pampeanas. Revista de la Asociación Geológica Argentina 70 (3), 427–435.
Ludwig, K.R., 2003. Isoplot/Ex Version 3.0: A Geochronological Toolkit for Microsoft Excel. Berkeley Geochronology Center Special Publication. Vol. 4.
Malvin, D.J., Drake, M.J., 1987. Experimental determination of crystal/melt partitioning of Ga and Ge in the system forsterite-anorthite diopside. Geochimica et Cosmochimica Acta 51, 2117–2128.
Martin, R.F., 2006. A-type granites of crustal origin ultimately result from open-system fenitization-type reactions in an extensional environment. Lithos 91, 125–136.
Merino Martínez, E., Villaseca, C., Orejana, D., Pérez-Soba, C., Belousova, E., Andersen, T., 2014. Tracing magma sources of three different S-type peraluminous granitoid series by in situ U–Pb geochronology and Hf isotope zircon composition: the Variscan Montes de Toledo batholith (central Spain). Lithos 200-201, 273–298.
Milisenda, C.C., Liew, T.C., Hofmann, A.W., Köler, H., 1994. Nd isotopic mapping of the Sri Lankan basement: update, and additional constraints from Sr isotopes. Precambrian Research 66, 95–110.
Miller, H., Söllner, F., 2005. The Famatina complex (NW-Argentina): back-docking of an island arc or terrane accretion? Early Palaeozoic geodynamics at the western Gondwana margin. In: Vaughan, A.P.M., Leat, P.T., Pankhurst, R.J. (Eds.), Terrane Processes at the Margins of Gondwana. Geological Society of London. Special Publications. Vol. 246, pp. 241–256.
Miller, C.F., Stoddard, E.F., Bradfish, L.J., Dollase, W.A., 1981. Composition of plutonic muscovite: genetic implications. Canadian Mineralogist 19, 25–34.
Miller, C.F., McDowell, S.M., Mapes, R.W., 2003. Hot and cold granites? Implications of zircon saturation temperatures and preservation of inheritance. Geology 31, 529–532.
Miyashiro, A., 1978. Nature of alcalic volcanic rock series. Contributions to Mineralogy and Petrology 66, 91–104.
Nelson, D.R., 1992. Isotopic characteristic of potassic rocks. Evidence for the involvement of subducted sediment in magma genesis. Lithos 28, 403–420.
Otamendi, J.E., Ducea, M., Bergantz, G., 2012. Geological, petrological and geochemical evidence for progressive construction of an arc crustal section, Sierra de Valle Fértil, Famatinian arc, Argentina. Journal of Petrology 53 (4), 761–800.
Pankhurst, R.J., Rapela, C.W., Saavedra, J., Baldo, E.G., Dahlquist, J.A., Pascua, I., Fanning, C.M., 1998. The Famatinian arc in the central Sierras Pampeanas: an early to mid-Ordovician continental arc on the Gondwana margin. In: Pankhurst, R.J., Rapela, C.W. (Eds.), The Proto-Andean Margin of Gondwana. Geological Society of London. Special Publications Vol. 142, pp. 343–367.
Pankhurst, R.J., Rapela, C.W., Fanning, C.M., 2000. Age and origin of coeval TTG, I and S-type granites in the Famatinian belt of NW Argentina. Transactions of the Royal Society of Edinburgh, Earth Science 91, 151–168.
Papoutsa, A., Piper, G.P., Piper, D.J.W., 2015. Systematic mineralogical diversity in A-type granitic intrusions: control of magmatic source and geological processes. The Geological Society of America Bulletin, B31245.1 128 (3–4), 487–501.
Patiño Douce, A.E., 1997. Generation of metaluminous A-type granitoids by low-pressure melting of calc-alkaline granitoids. Geology 25, 743–746.
Patiño Douce, A.E., 1999. What do experiments tell us about the relative contributions of crust and mantle to the origin of granitic magmas? In: Castro, A., Fernández, C., Vigneresse, J.L. (Eds.), Understanding Granites. Geological Society of London, Special Publications. Vol. 168, pp. 55–75
Rämö, O.T., Dall'Agnol, R., Macambira, M.J.B., Leite, A.A.S., de Oliveira, D.C., 2002. 1.88 Ga oxidized A-type granites of the Rio Maria region, eastern Amazonian craton, Brazil: positively anorogenic! Journal of Geology 110, 603–610.
Ramos, V.A., Cristallini, E.O., Perez, D.J., 2002. The Pampean flat-slab of the Central Andes. Journal of South American Earth Sciences 15, 59–78.
Rapela, C.W., Pankhurst, R.J., Casquet, C., Baldo, E., Saavedra, J., Galindo, C., Fanning, C.M., 1998. The Pampean orogeny of the southern proto-Andes: evidence for Cambrian continental collision in the Sierras de Córdoba. In: Pankhurst, R.J., Rapela, C.W. (Eds.), The Proto-Andean Margin of South America. Geological Society of London, Special Publication. Vol. 142, pp. 182–217.
Rapela, C.W., Baldo, E.G., Pankhurst, R.J., Saavedra, J., 2002. Cordieritite and Leucogranite formation at low pressure: the El Pilón Granite Complex (Sierras Pampeanas, Argentina). Journal of Petrology 43, 1003–1028.
Rapela, C.W., Pankhurst, R.J., Casquet, C., Fanning, C.M., Baldo, E., González-Casado, J.M., Galindo, C., Dahlquist, A., 2007. The Río de la Plata craton and the assembly of SW Gondwana. Earth-Science Reviews 83, 49–82.
Rapela, C.W., Pankhurst, R.J., Dahlquist, J.A., Baldo, E.G., Casquet, C., Galindo, C., 2008a. Revisiting accretionary history and magma sources in the Southern Andes: time variation of "typical Andean granites". International Symposium on Andean Geodynamics, 7th, Nice, France, Extended Abstracts, pp. 427–430.
Rapela, C.W., Baldo, E.G., Pankhurst, R.J., Fanning, C.M., 2008b. The Devonian Achala batholith in the Sierras Pampeanas: F-rich aluminous A-type granites. San Carlos de Bariloche, Argentina South American Symposium on Isotope Geology, 6th, CDROM, Extended Abstract, p. 53.
Sawka, W.N., Heizler, M.T., Kistler, R.W., Chappell, B.W., 1990. Geochemistry of highly fractionated I- and S-type granites from the tin–tungsten province of western Tasmania. In: Stein, H.J., Hannah, J.L. (Eds.), Ore Bearing Systems; Petrogenesis and Mineralizing Processes. US Geol. Surv. Spec. Pap. Vol. 246, pp. 161–179.
Schwartz, J., Gromet, L., Miró, R., 2008. Timing and duration of the calc-alkaline arc of the Pampean orogeny: implications for the Late-Neoproterozoic to Cambrian evolution of Western Gondwana. Journal of Geology 116, 39–61.
Shabani, A.A.T., Lalonde, A.E., Whalen, J.B., 2003. Composition of biotite from granitic rocks of the Canadian Appalachian orogen; a potential tectonomagmatic indicator? The Canadian Mineralogist 41, 1381–1396.
Shand, S.J., 1927. The Eruptive Rocks. John Wiley, New York (360pp.).
Shellnutt, J.G., Zhou, M.F., 2007. Permian peralkaline, peraluminous and metaluminous A-type granites in the Panxi district, SW China: their relationship to the Emeishan mantle plume. Chemical Geology 243, 286–316.
Siegesmund, S., Steenken, A., López de Luchi, M.G., Wemmer, K., Hoffmann, A., Mosch, S., 2004. The Las Chacras-Potrerillos batholith (Pampean Ranges, Argentina): structural evidence, emplacement and timing of the intrusion. International Journal of Earth Sciences 93, 23–43.
Sims, J.P., Ireland, T.R., Camacho, A., Lyons, P., Pieters, P.E., Skirrow, R.G., Stuart Smith, P.G., 1998. U–Pb, Th-Pb and Ar-Ar geochronology from the southern Sierras Pampeanas, Argentina: implications for the Palaeozoic tectonic evolution of the western Gondwana Margin. In: Pankhurst, R.J., Rapela, C.W. (Eds.), The Proto-Andean Margin of Gondwana. Geological Society of London, Special Publications. Vol. 142, pp. 259–285.
Sosic, M.V., 1972. Descripción Geológica de la Hoja 14d, Tinogasta, Provincias de Catamarca y La Rioja. Subsecretaría de Minería de Buenos Aires.
Streckeisen, A., 1976. To each plutonic rock its proper name. Earth Science Reviews 12, 1–33.
Stuart-Smith, P.G., Miró, R., Sims, J.P., Pieters, P.E., Lyons, P., Camacho, A., Skirrow, R.G., Black, L.P., 1999. Uranium-lead dating of felsic magmatic cycles in the southern Sierras Pampeanas, Argentina: implications for the tectonic development of the proto-Andean Gondwana margin. In: Ramos, V.A., Keppie, J.D. (Eds.), Laurentia Gondwana Connections before Pangea. Geological Society of America, Special Publication. Vol. 336, pp. 87–114.
Sun, S.S., McDonough, W.F., 1989. Chemical and isotopic systematics of oceanic basalts; implications for mantle composition and processes. In: Saunders, A.D., Norry, M.J.

(Eds.), Magmatism in the Ocean Basins: Geological Society of London. Special Publications. Vol. 42, pp. 313–345.
Sun, Y., Ma, C., Liu, Y., She, Z., 2011. Geochronological and geochemical constraints on the petrogenesis of late Triassic aluminous A-type granites in southeast China. Journal of Asian Earth Sciences 42, 1117–1131.
Tang, M., Wang, X.L., Shu, X.J., Wang, D., Yang, T., Gopon, P., 2014. Hafnium isotopic heterogeneity in zircons from granitic rocks: geochemical evaluation and modeling of "zircon effect" in crustal anatexis. Earth and Planetary Science Letters 389, 188–199.
Taylor, S.R., McLennan, S.M., 1985. The Continental Crust: Its Composition and Evolution. Blackwell Scientific Publications, Great Britain, p. 312.
Toselli, A., Bossi, G., Avila, J.C., Miró, R., Sesma, P., Durand, F., Rossi de Toselli, J., Cisterna, C., López, J.P., Sardi, F., Saavedra, J., Córdoba, G., Guido, E.y., Puchulu, M.E., 2014. Hoja Geológica 2966-I, Aimogasta; provincias de La Rioja y Catamarca. 1:250.000. Boletín Nº 421. IGRM-SEGEMAR. Buenos Aires.
Toselli, G.A., Saavedra, J., Córdoba, G., Medina, M.E., 1992. Los granitos peraluminosos de las sierras de Vinquis, cerro Negro y Zapata (Sierras Pampeanas), provincia de Catamarca, Argentina. Estudios Geológicos 48, 247–256.
Vallinayagam, G., Kochhar, N., 2011. Petrological Evolution and Emplacement of Siwana and Jalor Ring Complexes of Malani Igneous Suite, Northwestern Peninsular India. In: Ray, J., Sen, G., Ghosh, B. (Eds.), Topics in Igneous Petrology. Springer, Heidelberg, pp. 437–448.
Villaros, A., Buick, I.S., Stevens, G., 2012. Isotopic variations in S-type granites: an inheritance from a heterogeneous source? Contributions to Mineralogy and Petrology 163, 243–257.
Villaseca, C., Pérez Soba, C., Merino, E., Orejana, J., López García, J.A., Billstrom, K., 2008. Contrasting crustal sources for peraluminous granites of the segmented Montes de Toledo Batholith (Iberian Variscan Belt). Journal of Geosciences 53, 263–280.
Wang, C., Chen, L., Bagas, L., Lu, Y., He, X., Lai, X., 2015. Characterization and origin of the Taishanmiao aluminous A-type granites: implications for Early Cretaceous lithospheric thinning at the southern margin of the North China craton. International Journal of Earth Sciences 1–27.
Watson, E.B., 1996. Dissolution, growth and survival of zircons during crustal fusion: kinetic principles, geological models and implications for isotopic inheritance. Transactions of the Royal Society of Edinburgh: Earth Sciences 87, 43–56.
Watson, E.B., Harrison, T.M., 1983. Zircon saturation revisited: temperature and composition effects in a variety of crustal magma types. Earth and Planetary Science Letters 64, 295–304.
Whalen, J.B., Currie, K.L., Chappell, B.W., 1987. A-type granites: geochemical characteristics, discrimination and petrogenesis. Contributions to Mineralogy and Petrology 95, 407–419.
Whitney, D.L., Evans, B.W., 2010. Abbreviations for names of rock-forming minerals. American Mineralogist 95, 185–187.
Williamson, B.J., Shaw, A., Downes, H., Thirlwall, M.F., 1996. Geochemical constraints on the genesis of Hercynian two-mica leucogranites from the Massif Central, France. Chemical Geology 127, 25–42.
Wilson, M., 1989. Igneous Petrogenesis: A Global Tectonic Approach. Chapman & Hall, London.
Wolf, M.B., London, D., 1994. Apatite dissolution into peraluminous haplogranitic melts: an experimental study of solubilities and mechanisms. Geochimica et Cosmochimica Acta 58 (19), 4127–4146.
Wolf, M.B., London, D., 1995. Incongruent dissolution of REE and Sr-rich apatite in peraluminous granitic liquids: differential apatite, monazite, and xenotime solubilities during anatexis. American Mineralogist 80 (7–8), 765–775.
Xia, Y., Xu, X.S., Zhu, K.Y., 2012. Paleoproterozoic S- and A-type granites in southwestern Zhejiang: magmatism, metamorphism and implications for the crustal evolution of the Cathaysia basement. Precambrian Research 216-219, 177–207.
Zen, E., 1986. Aluminum enrichment in silicate melts by fractional crystallization: some mineralogic and petrographic constraints. Journal of Petrology 27, 1095–1117.
Zen, E., 1988. Phase relations of peraluminous granitic rocks and their petrogenetic implications. Annual Review of Earth and Planetary Sciences 16, 21–51.